Imperial College London

Department of Electrical and Electronic Engineering

RIS-aided Dual-Functional Radar and Communications Beamforming Design

Student:
Zhaolin Wang

Supervisor:
Prof Bruno Clerckx

A thesis submitted in fulfillment of requirements for the degree of

Master of Science

Communications and Signal Processing

September 2, 2021

Abstract

The development of the radar system, which has been widely used since the last century, is hindered by interference from the next-generation wireless communication system due to the spectrum scarcity problem. Dual-functional radar and communication (DFRC) system, where the radar and communication systems are jointly deployed in a single hardware platform and working simultaneously, is recognized as a promising solution to this problem. However, the achievable region of radar and communication performance is limited by the capability of base station (BS). Thus, in this project, we proposed the deployment of reconfigurable intelligent surface (RIS) in DFRC system to enlarge the achievable region. The RIS is capable of intelligently controlling the propagation environment of electromagnetic wave by adjusting the magnitude and phase of its reflecting elements.

Specifically, in this project, we investigated the joint optimization of passive beamforming at RIS and active beamforming at a dual-functional BS with separated or shared deployment. In order to maximize the Weighted Sum Rate (WSR) at communication users and probing power at target simultaneously, we proposed two alternating optimization (AO) methods based on Weighted Minimum Mean Square Error (WMMSE) framework and Fractional Programming (FP) for separated and shared deployments. Unlike many works of literature considering single connected RIS model, a generalized group or fully connected RIS model is exploited in this project. Simulation results demonstrate that RIS can help to achieve better transmission beampattern, improve WSR upper bound, and enlarge the achievable region.

Acknowledgements

First and foremost, I would want to convey my gratitude to Prof. Bruno Clerckx, my supervisor. His continuous help and valuable suggestions have been crucial for this research project. I also want to thank Mr. Rafael Cerna Loli, who was always open to answer my questions.

In this difficult time of COVID-19, I would like to thank my friends from Imperial College London and other universities for their support. Their company in the most difficult moments makes my life not lonely.

Finally, I want to express my love to my parents. Their selfless support and encouragement have been my biggest motivation in the past year.

Contents

List of Figures

List of Tables

Chapter 1

Introduction

1.1 Background

In the current 4G and 5G communication system, the spectrum band utilized is competing with that of the radar system below 10 GHz, leading to severe spectrum congestion and hinder the performance of both future communication and radar system [3]. Communications and Radar Spectrum Sharing (CRSS) was proposed to enable the two systems to perform in the same frequency band with tiny performance loss, which is regarded as the long-term solution for the spectrum management of communications and radar [4, 5]. Designing a dual-functional radar and communication (DFRC) system is one of the most popular aspects of the literature.

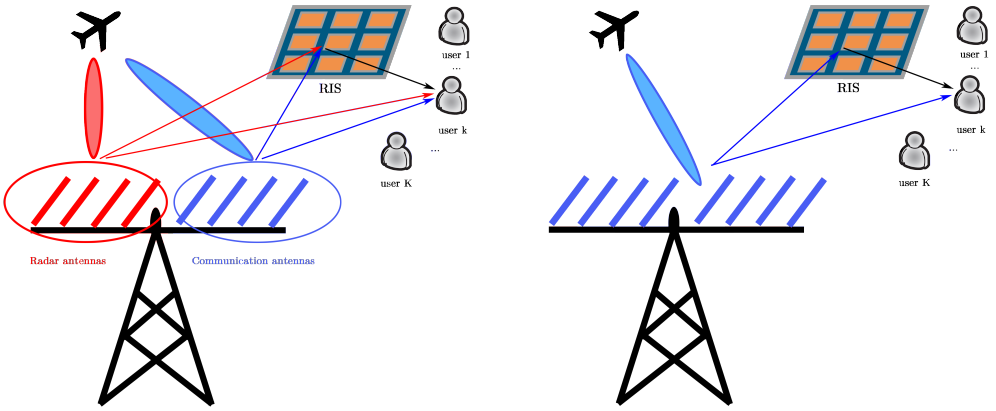

(a) Separated Deployment (b) Shared Deployment

Figure 1.1: RIS-aided Dual-functional Radar and Communication system

Meanwhile, there is a high requirement of spectral efficiency (SE) and high energy efficiency (EE) in next-generation (NG) communication networks due to the rapid expansion of modern techniques such as multimedia and the Internet of Things (IoT). In the past decade, Reconfigurable Intelligent Surface (RIS) is proposed as a potential technique to satisfy the SE and EE requirement. RIS consists of many small reflecting elements, which can change the amplitude and/or phase of the electromagnetic waves to achieve the desired propagation characteristics [1]. These reflecting elements are normally low-cost. The reflecting coefficients (passive beam-

forming) at RIS can be controlled by the base station (BS) through the controllers. Therefore, in order to maximize the gain from RIS, the beamforming at BS and RIS are usually designed jointly. [6, 7, 8].

In the DFRC system, there is usually a tradeoff between the radar and communications [9], which means the performance of radar needs to be decreased to increase the performance of communications, and vice versa. The RIS is capable of modifying the communication channel via passive beamforming, which can provide extra capability for the communication functions in the DFRC system. Compared with the DFRC without RIS, the RIS-aided DFRC has more capability (passive beamforming) to achieve better communication performance when the radar performance is the same. Meanwhile, because of the tradeoff relationship, when the communication performance is the same, better radar performance can also be achieved in RIS-aided DFRC. Therefore, by optimizing the active beamforming and passive beamforming, the overall performance of DFRC can be enhanced.

1.2 Literature Review

1.2.1 Communications and Radar Spectrum Sharing

CRSS is the technique that allows the communications and radar systems to work in the same frequency band. It can be categorized into coexistence and co-design

CRSS is motivated by solving the coexistence problem of radar and communication systems [5]. In the coexistence cases, the most significant issue is the interference cancellation, so that the two systems can work without imposing interference on each other. Many methods have been investigated, such as optimizing the beamforming [10, 11, 12, 13, 14], nulling interference at transmitter [15, 16], and adaptively eliminating interference at the receiver [17, 18, 19].

Co-design is to integrate the two systems into a single platform and design a dual-functional radar and communications (DFRC) system, where target sensing and communication can be performed simultaneously [20]. There are two methods to achieve it: radar- and communication-centric.

The main idea of radar-centric DFRC is embedding the information into the radar waveform, without interfering with the radar function. For example, the information can be embedded using beamforming modulation and index modulation [20]. Hassanien et al. [21] considered the two-way communication where the communication information is embedded in the radar signal emitting in the direction of users. However, the rate of communications is restricted by the pulse repetition frequency (PRF) of radar, because each radar pulse can only support a small number of communication symbols [22].

In communication-centric DFRC, the target data is extracted from the echoed communication waveform. All the commonly-used communication waveforms can be used for this task [4]. As opposed to the radar-centric method, the communication-centric method is capable of supporting a higher communication rate and guaranteeing radar performance by carefully designing the waveform [22]. Therefore, in this project, we mainly focus on waveform design for communication-centric DFRC.

Many works have been done in the field of communication-centric DFRC [9, 22, 23]. For example, in [23], Liu et al. designed a DFRC platform that supports probing several radar targets and serving several communication users simultaneously. Specifically, two platform deployments were proposed: separated deployment and shared deployment. In the former, the antennas are separated into two groups and each group performs radar or communication function, while shared deployment only transmits communication waveform which is designed to approximate a pre-designed beampattern or 3dB-main beamwidth. The shared deployment was also considered in [22], but an additional jointly precoded radar waveform is added on communication waveform to maximize the degree of freedom (DoF) of radar. Apart from achieving the desired beampattern, the waveform was also designed to minimize the mean-squared cross-correlation, which can suppress the interference from undesired targets. However, in both [23] and [22], the SINR was used as the communication metric, instead of more representative metrics like weighted sum rate (WSR). Xu et al. [9] first considered WSR maximization in DFRC context, where the tradeoff between probing power at target and WSR were investigated. Compared with beampattern approximation in [23] and [22], probing power maximization lead to clearer tradeoff comparison. Thus, the probing power at target and WSR were used as radar and communication metrics in this project.

1.2.2 Reconfigurable Intelligent Surface

As was aforementioned, many works considered the joint beamforming design for RIS-aided communication system [6, 7, 8]. Specifically, a RIS-aided wireless communication was investigated in [7], where both single- and multiple-user cases are considered. With the additional RIS-aided channel between BS and users, the authors tried to use as low transmit power as possible but guaranteed the SINR at users. Numerical results indicate that the number of RF chains can be significantly reduced in a RIS-aided MIMO system when the performance is the same as massive MIMO. Similarly, WSR is also more representative than SINR in the context of RIS-aided communication system. Therefore, Guo et al. [6] first studied the maximization of WSR for all users in the context of RIS-aided communication system. To solve the non-convex and NP-hard WSR maximization problem, an algorithm using fractional programming (FP) [24, 25] and alternating optimization (AO) was proposed. The work [8] extended the method of [6], where the beamformings are jointly designed to maximize the WSR with imperfect channel state information (CSI).

Recently, RIS also shows benefits in aiding radar system [26, 27, 28, 29]. In [26], the active beamforming for target detection at MIMO radar and passive beamforming at a co-located RIS are optimized separately, in order to increase the detection performance. A RIS-aided detection algorithm was also proposed and it is shown that RIS can result in better Cramér–Rao bound (CRB). Unlike [26] wherein the RIS helps to receive the reflected signal at radar receiver, Buzzi et al. [27] designed a system wherein the radar transmits or receives through two beams, one towards the target and another towards RIS. It is theoretically proved that RIS can provide improvement to received SNR by phase-aligning the echo signals no matter the radar and RIS are closely- or widely-spaced. When the LOS between radar

and target is blocked, an artificial path can be established via RIS. Aubry et al. [28] investigated this scenario by discussing the data acquisition, resolution issues of estimated parameters, and size and system parameters of RIS. By considering all the aforementioned RIS-aided scenarios, a general signal model was introduced in [29], which can cover the following conditions: one or two RIS's, mono-static or bi-static radar configuration, and with or without LOS. They also optimized the passive beamforming at RIS to improve the detection probability with the fixed false-alarm probability.

In most existing investigations about RIS-aided systems, including the aforementioned ones, the single connected reconfigurable impedance network is widely applied to model the RIS. Recently, Shen et al. [2] proposed a generalized model in which the RIS network is group or fully connected. This novel model significantly outperforms the single connected RIS network in terms of received power. This project also investigated the potential benefits of this generalized RIS model in the RIS-aided DFRC system.

1.2.3 RIS-aided DFRC

The RIS-aided DFRC system is still an open research area with few works [30, 31, 32]. Wang et al. [30] first investigate a RIS-aided radar-communication coexistence, where the radar detection probability is maximized by optimizing active and passive beamforming and the received SINR at communication users is guaranteed. It was proved that the detection probability maximization problem can be relaxed to a interference minimization problem of received echos at radar. In [31], the DFRC system is first considered. Similarly, the SINR of echos is maximized under users' SINR constraints. A two-stage algorithm was designed for the non-convex joint beamforming optimization and the improvement of SINR in both radar and communication. RIS-aided DFRC system was also studied in [32]. Unlike the previous two works, the beamforming is designed to form a pre-designed beampattern and eliminate the multi-user interference (MUI). The tradeoff between radar and communication performance was also investigated. Nevertheless, as mentioned before, WSR is a more representative metric than SINR and MUI in the context of both DFRC and RIS-aided system. Thus, in this project, the objective is to maximize the WSR at users in RIS-adied DFRC system.

1.3 Objectives and Methodology

In this project, we aim to design a RIS-aided multi-antenna DFRC system and jointly design active beamforming at a dual-functional BS and passive beamforming at RIS to maximize the WSR at users and probing power at target simultaneously.

As was aforementioned, there are only a few works in the field of RIS-aided DFRC [30, 31, 32], and we explore different communication and radar metrics (i.e., WSR and probing power) in this project. According to the qualitative analysis in Section 1.1, a larger achievable region of DFRC system can be realized with RIS. In the following sections, the quantitative results will be given. Two deployments of

dual-functional BS, separated and shared deployments [9, 23], are both considered. In both deployments, the joint active and passive beamforming design is converted to an optimization problem and solved in an alternative manner. The impact of generalized RIS model [2] over DFRC system is compared with conventional single-connected RIS model in terms of WSR and probing power enhancement in both Rayleigh and LOS channels.

1.4 Contributions

In this project, we propose an RIS-aided DFRC active and passive beamforming desgin, which enable communicating with the downlink users and probing target in an interesting direction in both separated and shared deployments. The following is a list of the project's major contributions.

1. We propose a joint beamforming design at BS and RIS that maximizes WSR and the probing power at target for both separated and shared deployment. To our knowledge, this is the first study of WSR maximising for a RIS-aided DFRC system. As in [9], we also consider probing power as radar metric to make a clear tradeoff comparison. However, the logarithm form and additional radar signal term of WSR, the quadratic form of probing power, and the quadratic equality power constraint make the optimization of joint beamforming rather non-convex and elusive.

2. This is also the first work that investigates the novel group or fully connected RIS model in RIS-aided DFRC. This novel RIS model is capable of enhancing the SNR performance especially in the Rayleigh fading channel [2], but its potential benefits for enlarging achievable region of WSR and probing power in DFRC are studied in this project.

3. We propose an AO algorithm for the proposed non-convex design in separated deployment. As was proposed in [9], the active beamforming problem is reformulated to a semidefinite programming (SDP) problem using WMMSE framework. The passive beamforming problem is reformulated to an unconstrained problem based on Lagrangian dual transform [25], quadratic transform [24], and scattering-reactance relationship [2]. Compared with the passive beamforming optimization method in [6], this method is an extended version that considers an additional radar signal term and generalized RIS model.

4. We propose another AO algorithm to solve the non-convex design for shared deployment. The optimal active beamforming can be obtained by WMMSE framework and semidefinite relaxation (SDR) [33]. In contrast to the majorization-minimization (MM) method used in [9], which requires several steps to reach the optimal values, this SDR method only needs one step and therefore has lower complexity. The passive beamforming is optimized using the same method as separated deployment.

1.5 Organization

The rest of this report is organized as follows:

- Chapter 2 introduces the theoretical background of this project, including wireless communication system, MIMO radar, and reconfigurable intelligent surface.
- In Chapter 3, the system model and formulated problems are given. The detailed optimization methods for joint active and passive beamforming are presented. Both separated and shared deployments are considered.
- In Chapter 4, we discuss the simulation results, including the convergence of proposed algorithms, beampattern comparison, and tradeoff comparison.
- In Chapter 5, the conclusions and potential future works are discussed.

Chapter 2

Background

2.1 Wireless Communication Systems

2.1.1 Discrete-time Baseband Wireless communication Model

The general discrete-time baseband wireless communication model is illustrated in Fig.2.1, which consists of three parts: transmitter, wireless channel, and receiver.

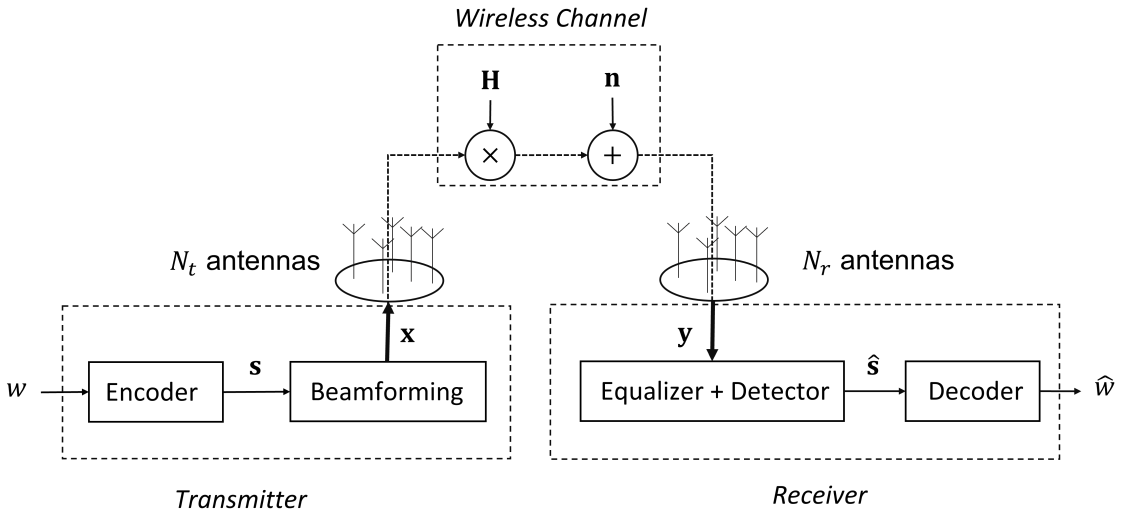

Figure 2.1: General discrete-time baseband wireless communication model

The wireless communication systems can be classified into:

- SISO (Single-Input Single-Output): $N_t = N_r = 1$;
- SIMO (Single-Input Multiple-Output): $N_t = 1, N_r > 1$;
- MISO (Multiple-Input Single-Output): $N_t > 1, N_r = 1$;
- MIMO (Multiple-Input Multiple-Output): $N_t > 1, N_r > 1$.

Let's firstly take SISO as an example. Without considering noise, the wireless channel is modeled as [34]

$$h(\tau, t) = \sum_i \beta_i(t)\delta(\tau - \tau_i(t)), \tag{2.1}$$

where $h(\tau, t)$ is the channel response at time t to an impulse transmitted at time $t - \tau$. Thus, the received signal for the transmitted $c(t)$ is

$$\begin{aligned} y(t) &= \int_{-\infty}^{\infty} h(\tau, t)c(t - \tau)d\tau \\ &= \sum_i \beta_i(t)c(t - \tau_i(t)). \end{aligned} \tag{2.2}$$

Since many operations in wireless communication system are at baseband, we usually transform the signal to baseband. The baseband equivalent of $y(t)$ is [34]

$$y_b(t) = \sum_i \beta_i^b c_b(t - \tau(t)), \tag{2.3}$$

where $\beta_i^b(t) = \beta_i(t)e^{-j2\pi f_c \tau_i(t)}$ with f_c denoting carrier frequency. $c_b(t)$ is the baseband equivalent of $c(t)$ and is defined as

$$c_b(t) = \frac{1}{\sqrt{2}}\Big(c(t) + \hat{c}(t)\Big)e^{-j2\pi f_c t}, \tag{2.4}$$

where $\hat{c}(t)$ is the Hilbert transform of $c(t)$. Thus, according to (2.3), the baseband channel response is

$$h_b(\tau, t) = \sum_i \beta_i^b \delta(\tau - \tau_i(t)). \tag{2.5}$$

For a digital system, the signal need to be sampled. From Shannon sampling theorem, if $c_b(t)$ is band-limited to $B/2$, it can be transformed as

$$c_b(t) = \sum_n c[n]\text{sinc}(Bt - n), \tag{2.6}$$

where $c[n] = c_b(n/B)$ is the sampled version of $c_b(t)$. By substituting (2.6) into (2.3), we have

$$y_b(t) = \sum_n c[n] \sum_i \beta_i^b(t)\text{sinc}(Bt - B\tau_i(t) - n). \tag{2.7}$$

The sampled version of $y_b(t)$ with $f_s = B$ is

$$\begin{aligned} y[k] &\coloneqq y_b\left(\frac{k}{B}\right) \\ &= \sum_n c[n] \sum_i \beta_i^b\left(\frac{k}{B}\right) \text{sinc}\left[k - n - B\tau_i\left(\frac{k}{B}\right)\right] \\ &\overset{\ell=k-n}{=} \sum_\ell c[k - \ell] \sum_i \beta_i^b\left(\frac{k}{B}\right) \text{sinc}\left[\ell - B\tau_i\left(\frac{k}{B}\right)\right] \end{aligned} \tag{2.8}$$

Therefore, the discrete-time baseband equivalent of channel response is

$$h_\ell[k] = \sum_i \beta_i^b \left(\frac{k}{B}\right) \text{sinc}\left[\ell - W\tau_i\left(\frac{k}{B}\right)\right]. \tag{2.9}$$

By considering the additive noise, the discrete-time baseband system model of wireless communication system is

$$y[k] = \sum_\ell h_\ell[k]c[k-\ell] + n[k]. \tag{2.10}$$

In flat fading, the channel is represented by a single channel filter tap [34]

$$y[k] = h[k]c[k] + n[k]. \tag{2.11}$$

We now expand the SISO case to a general one. By dropping the time index, the received signal for any amounts of antennas is

$$\mathbf{y} = \mathbf{H}\mathbf{c} + \mathbf{n}, \tag{2.12}$$

where $\mathbf{y} \in \mathbb{C}^{N_r \times 1}$, $\mathbf{H} \in \mathbb{C}^{N_r \times N_t}$, $\mathbf{c} \in \mathbb{C}^{N_t \times 1}$, and $\mathbf{n} \sim \mathcal{CN}(\mathbf{0}, \sigma_n^2 \mathbf{I}_{N_r})$.

When $N_t > 1$, beamforming, also called linear precoding, is usually exploited to eliminate the interference on each independent stream $s_i \in \mathbb{C}, i = 1, ..., R$ in the transmitted $\mathbf{s}$, by adjusting the gain and phase of the signal fed to each antenna. The beamforming matrix is denoted by $\mathbf{P} = [\mathbf{p}_1, ..., \mathbf{p}_R] \in \mathbb{C}^{N_t \times R}$. The received signal can be rewritten as

$$\mathbf{y} = \mathbf{H}\mathbf{P}\mathbf{s} + \mathbf{n} = \mathbf{H}\sum_{i=1}^{R} \mathbf{p}_i s_i + \mathbf{n}, \tag{2.13}$$

where $R \leq \text{rank}(\mathbf{H})$ and $\text{Tr}(\mathbf{P}\mathbf{P}^H) \leq P_t$. P_t is the power budget of transmitter.

At the receiver, the equalizer can also be used to minimize the interference. Let $\mathbf{g}_j \in \mathbb{C}^{1 \times N_r}$ denote the equalizer for j-th stream. The input of detector is given as

$$z_j = \mathbf{g}_j \mathbf{H} \sum_{i=1}^{R} \mathbf{p}_i s_i + \mathbf{g}_j \mathbf{n}. \tag{2.14}$$

Then, $\hat{s}_j$ is detected by the detector based on z_j.

2.1.2 Capacity of Wireless Channels

Capacity or achievable rate is one of the most representative metrics of a wireless communication system and gives the upper bound of the data rate that can be transmitted in a specific channel without any error.

The transmitted signal $\sqrt{E_s}x$ through additive white Gaussian noise (AWGN) channel is

$$y = \sqrt{E_s}x + n, \tag{2.15}$$

where E_s is transmit power, x satisfies $\mathbb{E}(|x|^2) = 1$ and $n \sim \mathcal{CN}(0, \sigma_n^2)$ is complex Gaussian noise. The AWGN channel capacity can be derived by Shannon information theory and is given as

$$C = \log_2(1 + \rho) \quad [\text{bits/s/Hz}], \tag{2.16}$$

where $\rho = E_s/\sigma_n^2$ is the signal-to-noise ratio (SNR).

However, in fading channel, the capacity is also determined by fading. The capacity in different fading is shown as follows [35]:

- **Deterministic SISO Channel**

$$\text{Received signal: } y = \sqrt{E_s}hc + n \tag{2.17}$$
$$\text{Capacity: } C = \log_2(1 + \rho|h|^2) \quad [\text{bits/s/Hz}] \tag{2.18}$$

- **Deterministic SIMO Channel**

$$\text{Received signal: } \mathbf{y} = \sqrt{E_s}\mathbf{h}c + \mathbf{n} \tag{2.19}$$
$$\text{Capacity: } C = \log_2(1 + \rho\|\mathbf{h}\|^2) \quad [\text{bits/s/Hz}] \tag{2.20}$$

  In SIMO channel, the capacity can be achieved by maximum ratio combination (MRC) at receiver, i.e.,

$$\mathbf{h}^H\mathbf{y} = \sqrt{E_s}\|\mathbf{h}\|^2 c + \mathbf{h}^H\mathbf{n} \tag{2.21}$$

- **Deterministic MISO Channel**

$$\text{Received signal: } y = \sqrt{E_s}\mathbf{h}\mathbf{w}c + n \tag{2.22}$$
$$\text{Capacity: } C = \log_2(1 + \rho\|\mathbf{h}\|^2) \quad [\text{bits/s/Hz}] \tag{2.23}$$

  In MISO channel, the capacity can be achieved by maximum ratio transmission (MRT) with perfect transmit channel knowledge, i.e., $\mathbf{w} = \mathbf{h}^H/\|\mathbf{h}\|$ and

$$y = \sqrt{E_s}\|\mathbf{h}\|c + n \tag{2.24}$$

- **Deterministic MIMO Channel**

$$\text{Received signal: } \mathbf{y} = \sqrt{E_s}\mathbf{H}\mathbf{c}' + \mathbf{n} \tag{2.25}$$
$$\text{Capacity: } C = \max_{\mathbf{Q}\geq 0:\mathrm{Tr}\{\mathbf{Q}\}=1} \log_2 \det\left[\mathbf{I}_{N_r} + \rho\mathbf{H}\mathbf{Q}\mathbf{H}^H\right] \quad [\text{bits/s/Hz}] \tag{2.26}$$

  where $\mathbf{Q} = \mathbb{E}(\mathbf{c}'\mathbf{c}'^H)$ is the covariance of transmitted signal. The capacity can be achieved by applying multiple eigenmode transmission and using water-filling algorithm to find the optimal $\mathbf{Q}^\star$.

2.2 MIMO Radar Systems

The MIMO radar has attracted the attention of researchers in the last decades, because of its advantages over standard phase-array radar in terms of [36]:

1. adaptive localization and detection techniques;
2. freely-chosen probing signal that can approximate a desired beampattern and minimize the cross-correlation.

A MIMO radar system model is shown in Fig.2.2. If the transmitter and receiver in radar system share the same hardware, it is mono-static radar, while it is classified as bi-static radar if they are separated.

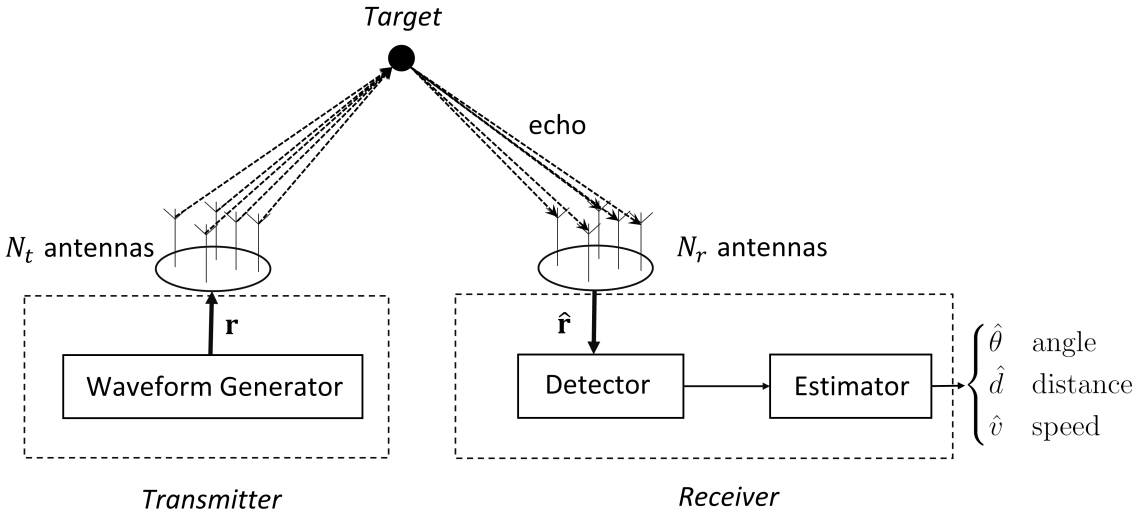

Figure 2.2: MIMO radar system model

2.2.1 Radar Waveform Design

The radar waveform **r** generated by the waveform generator should satisfy some radar-specific shaping constraints [4]:

1. *Low Sidelobe Level*: This is to reduce the interference from undesired directions. Generally, the probing power at target locations is maximized or the desired beampattern is achieved to satisfy this constraint.
2. *Low Peak-to-Average Power Ratio*: A radar system generally transmits signals at the maximum power budget to ensure the SNR of the echo signal is enough for detector. For the high power radar, the low peak-to-average power ratio is preferred to reduce to signal distortion. The optimal method is to use a constant-modulus waveform, i.e., the power fed to each antenna is the same.
3. *Clutter Suppression*: When there are multiple targets, the clutter interference is generated from undesired targets. In this case, the waveform should be

carefully designed to have small cross-correlation in different target directions [36].

The MIMO radar waveform can be designed to maximize the probing power in direction θ:

$$\max_{\mathbf{R}} \quad \mathbf{a}^H(\theta)\mathbf{R}\mathbf{a}(\theta) \tag{2.27a}$$

$$\text{s.t.} \quad \text{diag}(\mathbf{R}) = c\mathbf{1}_{N_t}, \tag{2.27b}$$

$$\mathbf{R} \succeq 0, \tag{2.27c}$$

where $\mathbf{a}(\theta) = [1, e^{j\frac{2\pi}{\lambda}d\sin(\theta)}, ..., e^{j\frac{2\pi}{\lambda}d(N_t-1)\sin(\theta)}]^T$ is the steering vector in direction of θ and $\mathbf{R} = \mathbb{E}(\mathbf{r}\mathbf{r}^H)$ is the covariance matrix of radar signal. In this design, the porbing power $\mathbf{a}^H(\theta)\mathbf{R}\mathbf{a}(\theta)$ is maximized under the constant-modulus constraint $\text{diag}(\mathbf{R}) = c\mathbf{1}_{N_t}$. More waveform designs for MIMO radar can be found in [36].

2.2.2 Radar Performance Metrics

There are two main tasks for a radar system: detection and estimation. Detection is to justify whether targets are present or not, while estimation is to extract target parameters, including angle, distance, and speed, from echo signals.

Detection

For detection problem, the binary hypothesis testing is normally applied [4]

$$\hat{\mathbf{r}}(t) = \begin{cases} \mathcal{H}_0: & \mathbf{z}(t), \\ \mathcal{H}_1: & \beta e^{2j\pi f_D t}\mathbf{s}_r(\varphi)\mathbf{s}_t^T(\varphi)\mathbf{r}(t-\tau) + \mathbf{z}(t). \end{cases} \tag{2.28}$$

There are two conditions in received signal $\hat{\mathbf{r}}(t)$:

- $\mathcal{H}_0$: only interference plus noise $\mathbf{z}(t)$.
- $\mathcal{H}_1$: echo signals $\beta e^{2j\pi f_D t}\mathbf{s}_r(\varphi)\mathbf{s}_t^T(\varphi)\mathbf{r}(t-\tau)$ and interference plus noise.

Specifically, β represents for the complex round-trip path loss and radar cross-section effect. $f_D = 2vf_c/c$ is the Doppler frequency. where v is the speed of target. $\mathbf{s}_r(\theta) \in \mathbb{C}^{N_r\times 1}$ and $\mathbf{s}_t(\theta) \in \mathbb{C}^{N_t\times 1}$ are receive and transmit steering vectors in direction of φ.

The final step of hypothesis testing is designing a detector $\mathcal{T}(\cdot)$ and then the output of detector is compared with a pre-set threshold τ

$$\mathcal{T}(\hat{\mathbf{r}}) \underset{\mathcal{H}_1}{\overset{\mathcal{H}_0}{\lessgtr}} \tau. \tag{2.29}$$

The radar performance are mainly evaluated by two metrics:

1. Detection probability P_D: target is present and detected by the radar.

2. False-alarm probability P_{FA}: target is not present but detected by the radar.

However, P_D and P_{FA} are usually complicated and not easy to be optimized. For this problem, a method is to relax them to a simple metric, which is shown in the following example.

Generalized likelihood ratio test (GLRT) is a popular method in detector. The detection probability in GLRT that determined by the Neyman-Pearson criterion is given as [30]:

$$P_D = 1 - \mathfrak{F}_{\mathcal{X}_2^2(\rho)}\Big(\mathfrak{F}_{\mathcal{X}_2^2}^{-1}(1 - P_{FA})\Big), \tag{2.30}$$

where $\mathfrak{F}_{\mathcal{X}_2^2(\rho)}$ is the non-central chi-square cumulative distribution function (CDF), and $\mathfrak{F}_{\mathcal{X}_2^2}^{-1}$ denotes the inverse operation. If the orthogonal radar signal is used, i.e., $\mathbf{R_r} = \mathbb{E}(\mathbf{r}\mathbf{r}^H) = P_R\mathbf{I}_{N_t}$, the parameter ρ is given as [30]:

$$\rho = |\beta|^2 P_R \mathrm{Tr}\Big(\mathbf{C}\mathbf{C}^H\mathbf{R}_\mathbf{z}^{-1}\Big), \tag{2.31}$$

where $\mathbf{C} = \mathbf{s}_r(\theta)\mathbf{s}_t^T(\theta)$ and $\mathbf{R_z} = \mathbb{E}(\mathbf{z}\mathbf{z}^H)$ is the covariance matrix of noise plus interference. The maximization problem of P_D can be converted to the maximization problem of ρ, because P_D is monotonically increasing with ρ. As the covariance matrix $\mathbf{R_z}$ is positive semidefinite, we have

$$\mathrm{Tr}\Big(\mathbf{C}\mathbf{C}^H\mathbf{R}_\mathbf{z}^{-1}\mathbf{R_z}\Big) \leq \mathrm{Tr}\Big(\mathbf{C}\mathbf{C}^H\mathbf{R}_\mathbf{z}^{-1}\Big)\mathrm{Tr}(\mathbf{R_z}) \tag{2.32}$$

$$\begin{aligned}
\Rightarrow \rho &= |\beta|^2 P_R \mathrm{Tr}\Big(\mathbf{C}\mathbf{C}^H\mathbf{R}_\mathbf{z}^{-1}\Big) \\
&\geq \frac{|\beta|^2 P_R \mathrm{Tr}\Big(\mathbf{C}\mathbf{C}^H\Big)}{\mathrm{Tr}(\mathbf{R_z})} \\
&= \frac{|\beta|^2 \mathrm{Tr}\Big(\mathbf{C}\mathbf{R_r}\mathbf{C}^H\Big)}{\mathrm{Tr}(\mathbf{R_z})} \\
&= \mathrm{SINR}_{\mathrm{echo}}
\end{aligned} \tag{2.33}$$

The parameter ρ is lower bounded by the SINR of the echo signal. Thus, the maximization problem of detection probability can be relaxed to the maximization problem of SINR of the echo signal.

Estimation

Once the target is detected, the target parameters, i.e., angle, distance, and speed, are extracted from $\mathbf{y}(t)$ by an estimator $\mathcal{F}(\cdot)$:

$$\mathcal{F}(\hat{\mathbf{r}}) = \{\hat{\theta}, \hat{d}, \hat{v}\}. \tag{2.34}$$

The estimator for each parameter is normally designed separately. For example, the angle can be estimated using subspace methods like MUltiple SIgnal Classification (MUSIC) [37]. The distance and speed can be estimated using matched-filtering algorithm [3].

Mean square error (MSE) between estimated and true values is an important metric to measure the estimator performance. However, the Cramér-Rao lower bound is normally used in practice because a closed-form MSE is difficult to derive.

2.3 Reconfigurable Intelligent Surface

RIS, which consists of an array of passive reflecting elements, is attracting many researchers and is regarded as a promising technique for NG wireless communications [1]. Due to its capability of intelligently reconfiguring the gain and phase of the signal, it can adjust the propagation environment for a wireless communication system and make improvements in terms of required power, achievable rate, SINR, etc.

2.3.1 System Model

Figure 2.3 depicts an example of a RIS-assisted wireless communication system.

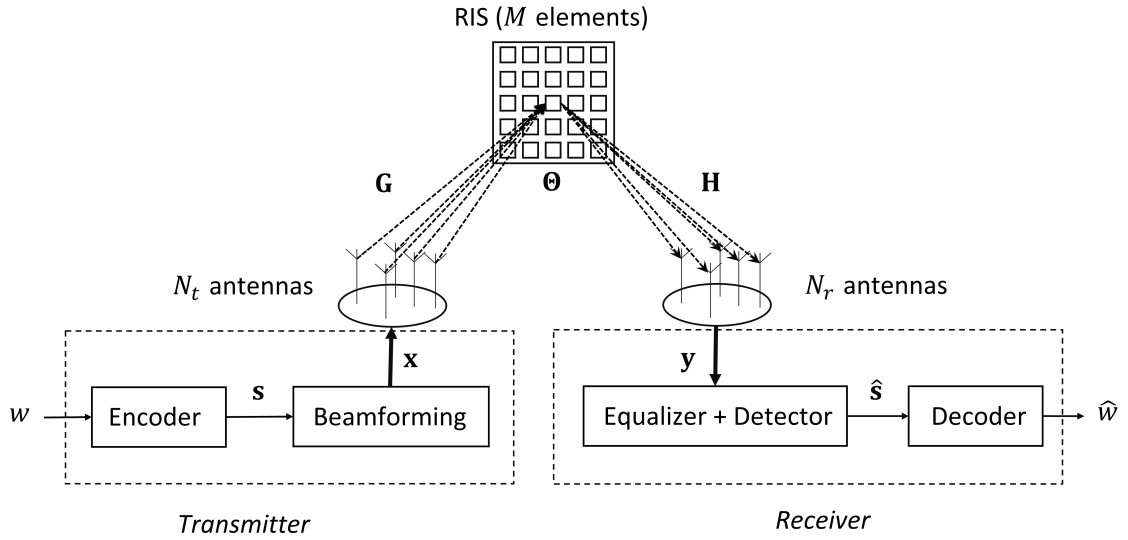

Figure 2.3: RIS-aided wireless communication system

Through the RIS-adied channel, the received signal is given as

$$\mathbf{y} = \mathbf{H\Theta Gx} + \mathbf{n} = \mathbf{H\Theta GPs} + \mathbf{n} = \underbrace{\mathbf{H\Theta G}}_{\tilde{\mathbf{H}}} \sum_{i=1}^{R} \mathbf{p}_i s_i + \mathbf{n}, \tag{2.35}$$

where $\mathbf{G} \in \mathbb{C}^{N_t \times M}$ denotes the channel between transmitter and RIS and $\mathbf{H} \in \mathbb{C}^{M \times N_r}$ denotes the channel between RIS and receiver. $\mathbf{\Theta} \in \mathbb{C}^{M \times M}$ is the reflecting matrix of RIS. Compared with (2.13), we can see that the efficient channel $\tilde{\mathbf{H}} = \mathbf{H\Theta G}$ in RIS-aided system can be adjusted by optimizing $\mathbf{\Theta}$, which is called passive beamforming. Generally, the active beamforming $\mathbf{P}$ and passive beamforming $\mathbf{\Theta}$ are jointly designed to maximize or minimize some communication metrics.

Now we consider an achievable rate maximization problem. For a MIMO system, the achievable rate is given as

$$R = \log_2 \det \left(\mathbf{I}_{N_r} + \frac{1}{\sigma_n^2} \tilde{\mathbf{H}} \mathbf{P} \mathbf{P}^H \tilde{\mathbf{H}} \right). \tag{2.36}$$

Thus, the problem of maximising the achievable rate can be phrased as

$$\max_{\mathbf{P},\mathbf{\Theta}} \quad R(\mathbf{P},\mathbf{\Theta}) \tag{2.37a}$$

$$\text{s.t.} \quad \text{Tr}(\mathbf{P}\mathbf{P}^H) \leq P_t, \tag{2.37b}$$

$$\mathbf{\Theta} \in \mathcal{Q}, \tag{2.37c}$$

where the first constraint stands for the power budget. $\mathcal{Q}$ denotes the feasible set of reflecting matrix $\mathbf{\Theta}$, which will be discussed in the next section.

2.3.2 Reconfigurable Intelligent Surface Model

In most literature, the RIS is modeled that each reflecting element works independently. Figure 2.4 shows the hardware model of RIS. Each element can be realized by a varactor diode, the equivalent load impedance of which can be adjusted by changing bias voltage [1]. In theory, each element can be characterized by the reflection coefficient

$$r = \beta e^{j\phi}, \tag{2.38}$$

where $\beta \in [0, 1]$ controls the gain and $\phi \in [0, 2\pi]$ controls the phase shift of reflected signal.

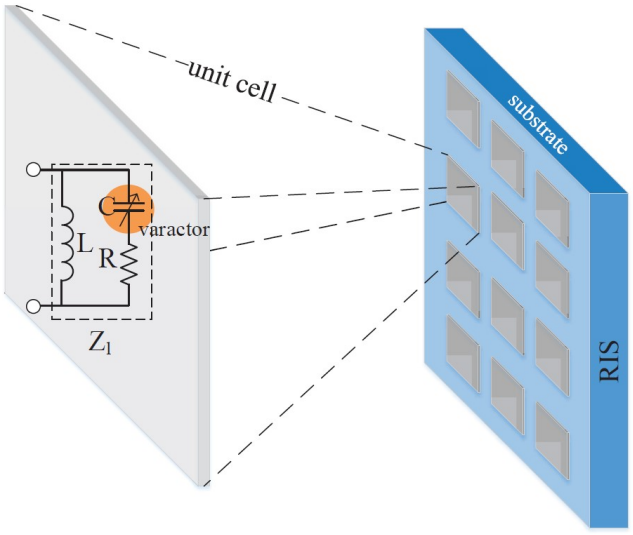

Figure 2.4: Hardware model of RIS [1]

As each element works independently in this model, the reflecting matrix $\mathbf{\Theta}$ in (2.35) is a diagonal matrix:

$$\mathbf{\Theta} = \text{diag}\left(\beta_1 e^{\phi_1}, \beta_2 e^{\phi_2}, ..., \beta_M e^{\phi_M}\right), \tag{2.39}$$

In this case, by letting $\theta_i = \beta_i e^{j\phi_i}$, the problem (2.37) can be written as

$$\max_{\mathbf{P},\mathbf{\Theta}} \quad R(\mathbf{P},\mathbf{\Theta}) \tag{2.40a}$$

$$\text{s.t.} \quad \text{Tr}(\mathbf{P}\mathbf{P}^H) \leq P_t, \tag{2.40b}$$

$$\mathbf{\Theta} = \text{diag}\left(\theta_1, \theta_2, ..., \theta_M\right), \tag{2.40c}$$

$$|\theta_i| \leq 1, \forall i. \tag{2.40d}$$

Recently, Shen el al. [2] proposed a novel RIS model (Figure 2.5 and 2.6) base on scattering parameter network analysis. In this novel model, the elements of RIS are group or fully connected instead of working independently, which shows advantages on received power in Rayleigh channel. The constraints of group and fully connected RIS model are given as

1. Grouped connected: $\mathbf{\Theta} = \text{diag}(\mathbf{\Theta}_1, \mathbf{\Theta}_2, ..., \mathbf{\Theta}_G), \mathbf{\Theta}_g = \mathbf{\Theta}_g^T, \mathbf{\Theta}_g^H \mathbf{\Theta}_g \preceq \mathbf{I}, \forall g$;
2. Fully connected: $\mathbf{\Theta} = \mathbf{\Theta}^T, \mathbf{\Theta}^H \mathbf{\Theta} \preceq \mathbf{I}$.

When the number of group G equals to 1, group connected RIS is equivalent to fully connected RIS; when G equals to the elements number M, group connected RIS is equivalent to single connected RIS, i.e., each element works independently.

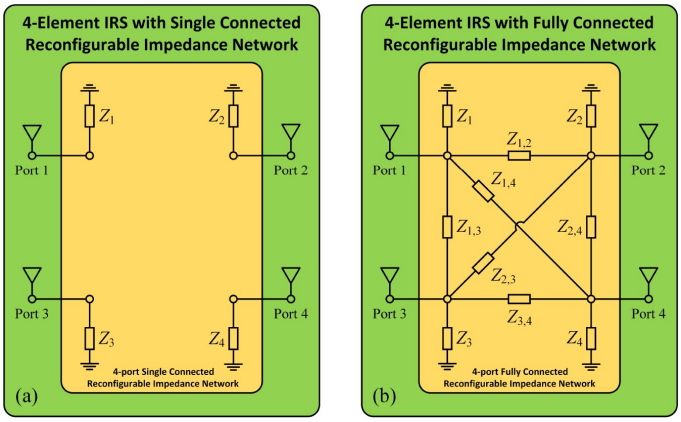

Figure 2.5: Model of single (a) and fully (b) connected RIS [2]

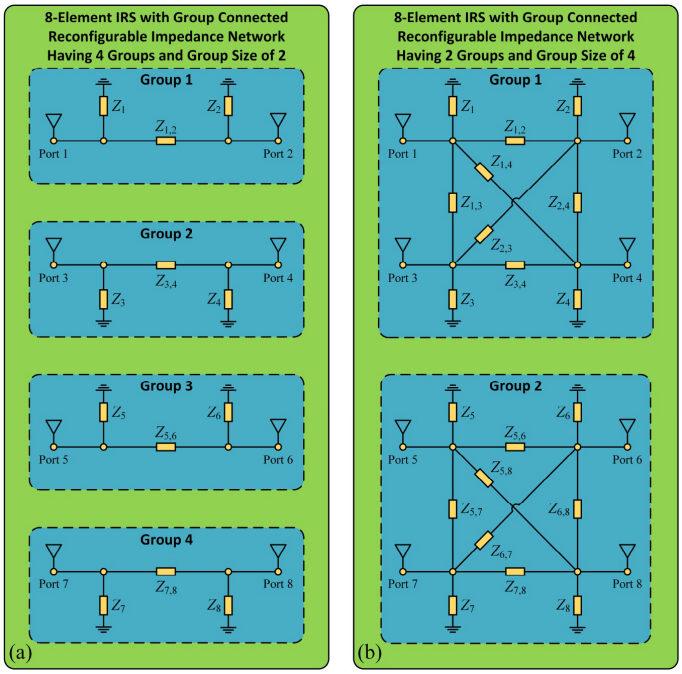

Figure 2.6: Model of group connected RIS[2]

Chapter 3

Joint Beamforming Design for RIS-aided DFRC system

In this section, the detailed design of joint active and passive beamforming for DFRC system is exposed, where the WSR and probing power at target are maximized simultaneously.

3.1 System Model

As shown in Figure 1.1, we aim to investigate the RIS-aided MIMO radar and MISO multi-user communications. This system serves K users with a signal antenna, which receives the signal from a BS equipped with M antennas and a RIS equipped with N reflecting elements. The uniform linear antennas (ULA) are assumed to be the antenna deployment in this model. The system also works in the tracking mode as a radar to tracking one target at the azimuth angle of φ_m. The overall power budget of this system is P. This system model partly follows the work [9].

3.1.1 Separated Deployment

In separated deployment, there are two groups of antennas: M_r radar antennas and M_c communication antennas, which transmit radar and communication signals separately. The power budgets of the radar and communications antennas are P_r and P_c, respectively.

The observation at user k is given as

$$x_k = (\mathbf{h}_k^H \mathbf{\Theta}^H \mathbf{H}_c + \mathbf{d}_{c,k}^H) \sum_{j=1}^{K} \mathbf{p}_j s_j + (\mathbf{h}_k^H \mathbf{\Theta}^H \mathbf{H}_r + \mathbf{d}_{r,k}^H)\mathbf{q} + n_k \tag{3.1}$$

where $\mathbf{h}_k \in \mathbb{C}^{N\times 1}$ is the channel from RIS to user k, $\mathbf{H}_c \in \mathbb{C}^{N\times M_c}$ and $\mathbf{H}_r \in \mathbb{C}^{N\times M_r}$ are the channels from communication and radar antennas to RIS, respectively. The direct channels from communication and radar antennas to user k are denoted by $\mathbf{d}_{c,k}$ and $\mathbf{d}_{r,k}$. s_j is the information symbol for user j, and $n_k \sim \mathcal{CN}(0, \sigma_n^2)$ is the complex Gaussian noise at user k. The linear precoding is exploited at the BS

and $\mathbf{p}_j \in \mathbb{C}^{M_c \times 1}$ is the linear precoder for user j. $\mathbf{q} \in \mathbb{C}^{M_r \times 1}$ is the radar signals whose covariance matrix is $\mathbf{R_q} = \mathbb{E}(\mathbf{q}\mathbf{q}^H)$. $\mathbf{\Theta} \in \mathbb{C}^{N \times N}$ is the (reflecting) passive beamforming matrix at RIS, which is modeled as group connected reconfigurable impedance network [2]:

$$\mathbf{\Theta} = \text{diag}(\mathbf{\Theta}_1, \mathbf{\Theta}_2, ..., \mathbf{\Theta}_G) \tag{3.2}$$

$$\mathbf{\Theta}_g = \mathbf{\Theta}_g^T, \mathbf{\Theta}_g^H \mathbf{\Theta}_g = \mathbf{I}, \forall g \tag{3.3}$$

where G is the number of groups in the impedance network and $\mathbf{\Theta}_g \in \mathbb{C}^{N_G \times N_G}$ is a full matrix. $N_G = N/G$ is the number of elements in each group. If $G = 1$, the RIS is a fully connected network; if $G = N$, the RIS is a single connected network.

The SINR and achievable rate at user k are

$$\gamma_k = \frac{|\mathbf{c}_k^H \mathbf{p}_k|^2}{\sum_{j=1, j \neq k}^{K} |\mathbf{c}_k^H \mathbf{p}_j|^2 + \mathbf{r}_k^H \mathbf{R_q} \mathbf{r}_k + \sigma_n^2} \tag{3.4}$$

$$R_k = \log_2(1 + \gamma_k) \tag{3.5}$$

where $\mathbf{c}_k = \mathbf{H}_c^H \mathbf{\Theta} \mathbf{h}_k + \mathbf{d}_{c,k}$ and $\mathbf{r}_k = \mathbf{H}_r^H \mathbf{\Theta} \mathbf{h}_k + \mathbf{d}_{r,k}$.

We aim to maximize the WSR as well as the probing power in direction φ_m. The WSR is given as

$$R = \sum_{k=1}^{K} \mu_k R_k \tag{3.6}$$

where μ_k is the weight specified for user k and is determined according the fairness and quality of service (QoS) requirements. The probing power in direction φ_m is given as

$$d(\varphi_m) = \mathbf{a}^H(\varphi_m) \mathbf{C} \mathbf{a}(\varphi_m) \tag{3.7}$$

where $\mathbf{a}(\varphi_m) \in \mathbb{C}^{M \times 1}$ is the steering vector. For ULA deployment, the steering vector is defined as

$$\mathbf{a}(\varphi_m) = [1, e^{j\frac{2\pi}{\lambda} d \sin(\varphi_m)}, ..., e^{j\frac{2\pi}{\lambda} d(M-1) \sin(\varphi_m)}]^T \tag{3.8}$$

where λ is the signal wavelength and d is the antenna spacing. Without loss of generality, we set $d = \lambda/2$. $\mathbf{C} \in \mathbb{C}^{M \times M}$ is the covariance matrix of the overall transmit signal. As the communication and radar signals are uncorrelated, the covariance matrix is given as

$$\mathbf{C} = \begin{bmatrix} \mathbf{R_q} & \mathbf{0} \\ \mathbf{0} & \mathbf{P}\mathbf{P}^H \end{bmatrix} \tag{3.9}$$

where $\mathbf{P} = \begin{bmatrix} \mathbf{p}_1, ..., \mathbf{p}_k \end{bmatrix}$

Therefore, (3.7) can be rewritten as

$$d(\varphi_m) = \mathbf{a}_r^H(\varphi_m) \mathbf{R_q} \mathbf{a}_r(\varphi_m) + \mathbf{a}_c^H(\varphi_m) \mathbf{P}\mathbf{P}^H \mathbf{a}_c(\varphi_m) \tag{3.10}$$

where $\mathbf{a}_r(\varphi_m)$ and $\mathbf{a}_c(\varphi_m)$ denote the steering vectors of radar and communication antennas, respectively.

3.1.2 Shared Deployment

In shared deployment, all the M antennas transmit communication signal. Therefore, the received signal at user k is

$$\check{x}_k = (\mathbf{h}_k^H \boldsymbol{\Theta}^H \mathbf{H} + \mathbf{d}_k^H) \sum_{j=1}^{K} \check{\mathbf{p}}_j s_j \tag{3.11}$$

where $\mathbf{h}_k \in \mathbb{C}^{N\times 1}$, $\mathbf{H} \in \mathbb{C}^{M\times N}$, $\mathbf{d}_k \in \mathbb{C}^M$, $\boldsymbol{\Theta} \in \mathbb{C}^{N\times N}$, $\check{\mathbf{p}}_j \in \mathbb{C}^{M\times 1}$, and $s_j \in \mathbb{C}$. The SINR at user k is

$$\check{\gamma}_k = \frac{|\check{\mathbf{c}}_k^H \check{\mathbf{p}}_k|^2}{\sum_{j=1,j\neq k}^{K} |\check{\mathbf{c}}_k^H \check{\mathbf{p}}_j|^2 + \sigma_n^2} \tag{3.12}$$

where $\check{\mathbf{c}}_k = \mathbf{H}^H \boldsymbol{\Theta} \mathbf{h}_k + \mathbf{d}_k$. Thus, the WSR is

$$\check{R} = \sum_{k=1}^{K} \mu_k \check{R}_k \tag{3.13}$$

where $\check{R}_k = \log_2(1 + \check{\gamma}_k)$ is the achievable rate at user k.

The probing power in direction of φ_m is

$$\check{d}(\varphi_m) = \mathbf{a}^H(\varphi_m) \sum_{j=1}^{K} \mathbf{p}_j \mathbf{p}_j^H \mathbf{a}(\varphi_m) \tag{3.14}$$

3.2 Problem Formulation

In this project, the perfect channel state information (CSI) is assumed to be known. The CSI acquisition is challenging in RIS-aided system because of the passive nature of RIS, which means it requires the estimation of a large number of unknown parameters cause by RIS [1]. However, this problem can be tackled by deep learning techniques such as deep denoising neural network [38] or convolutional neural network [39].

When CSI is known, the problem of transmission optimization and RIS optimization in separated deployment is formulated as

$$\max_{\mathbf{P},\mathbf{R_q},\boldsymbol{\Theta}} \quad \rho \sum_{k=1}^{K} \mu_k R_k(\mathbf{P}, \mathbf{R_q}, \boldsymbol{\Theta}) + \mathbf{a}_r^H(\varphi_m) \mathbf{R_q} \mathbf{a}_r(\varphi_m) + \mathbf{a}_c^H(\varphi_m) \mathbf{P}\mathbf{P}^H \mathbf{a}_c(\varphi_m) \tag{3.15a}$$

$$\text{s.t.} \quad \text{diag}(\mathbf{R_q}) = \frac{P_r}{M_r} \mathbf{1}^{M_r\times 1}, \tag{3.15b}$$

$$\text{Tr}(\mathbf{P}\mathbf{P}^H) \leq P_c, \tag{3.15c}$$

$$\mathbf{R_q} \succeq 0, \mathbf{R_q} = \mathbf{R_q}^H, \tag{3.15d}$$

$$\boldsymbol{\Theta} = \text{diag}(\boldsymbol{\Theta}_1, \boldsymbol{\Theta}_2, ..., \boldsymbol{\Theta}_G), \tag{3.15e}$$

$$\boldsymbol{\Theta}_g = \boldsymbol{\Theta}_g^T, \boldsymbol{\Theta}_g^H \boldsymbol{\Theta}_g = \mathbf{I}, \forall g, \tag{3.15f}$$

where the first part of (3.15a) is the WSR and the rest is the probing power in direction φ_m. Both of them are maximized with the regularization parameter ρ. (3.15b) is the constant-modulus constraint imposed by radar, so that the optimal low peak-to-average power ratio is guaranteed and the radar signal distortion is therefore reduced [4]. (3.15c) is the overall power budget constraint imposed by communications, and (3.15d) constraints the covariance matrix $\mathbf{R_q}$ to be Hermitian and positive semidefinite. The last two constraints are imposed by the RIS. After finding the optimal $\mathbf{R_q}$, the radar signal can be obtained by the method in [33].

In shared deployment, the dual-function optimization problem is formulated as

$$\max_{\check{\mathbf{p}}_1,...,\check{\mathbf{p}}_K} \quad \rho \sum_{k=1}^{K} \mu_k \check{R}_k(\check{\mathbf{p}}_1, ..., \check{\mathbf{p}}_K, \boldsymbol{\Theta}) + \mathbf{a}^H(\varphi_m) \sum_{k=1}^{K} \check{\mathbf{p}}_k \check{\mathbf{p}}_k^H \mathbf{a}(\varphi_m) \tag{3.16a}$$

$$\text{s.t.} \quad \text{diag}\left(\sum_{k=1}^{K} \check{\mathbf{p}}_k \check{\mathbf{p}}_k^H \right) = \frac{P}{M} \mathbf{1}^{M \times 1}, \tag{3.16b}$$

$$\boldsymbol{\Theta} = \text{diag}(\boldsymbol{\Theta}_1, \boldsymbol{\Theta}_2, ..., \boldsymbol{\Theta}_G), \tag{3.16c}$$

$$\boldsymbol{\Theta}_g = \boldsymbol{\Theta}_g^T, \boldsymbol{\Theta}_g^H \boldsymbol{\Theta}_g = \mathbf{I}, \forall g, \tag{3.16d}$$

where the WSR and probing power are also maximized with regularization parameter ρ. (3.16b) is the constant-modulus constraint for MIMO radar. The overall power constraint is omitted because it is obviously satisfied when the constant modulus is met. The last two constraints are for generalized RIS.

The problems (3.15) and (3.16) are essentially multi-objective optimization problems, which can lead to the tradeoff between different objectives, i.e., WSR and probing power.

3.3 WMMSE and Fractional Programming Based Algorithm

It is clear that both (3.15) and (3.16) are non-convex optimization problem. However, we point out that they can be converted to two optimization problems with respect to $\{\mathbf{P}, \mathbf{R}_x\}$ and $\boldsymbol{\Theta}$, respectively, using Weighted Minimum Mean Square Error (WMMSE) framework [40] and Fractional Programming (FP) [24]. Then the optimal solution can be obtained in an alternative manner.

3.3.1 Algorithm for Separated Deployment

WMMSE for Active Beamforming

Based on the WMMSE method proposed in [40], the WSR maximization problem in (3.15) can be converted to an equivalent weight mean square error (MSE) minimization problem via the following process.

The observation at user k can be rewritten as

$$\begin{aligned} x_k &= \mathbf{c}_k^H \sum_{j=1}^{K} \mathbf{p}_j s_j + \mathbf{r}_k^H \mathbf{q} + n_k \\ &= \mathbf{c}_k^H \mathbf{p}_k s_k + \underbrace{\mathbf{c}_k^H \sum_{j=1, j\neq k}^{K} \mathbf{p}_j s_j + \mathbf{r}_k^H \mathbf{q}}_{\text{interference}} + n_k. \end{aligned} \tag{3.17}$$

So the efficient noise plus interference power is

$$N_k = \sum_{j=1, j\neq k}^{K} |\mathbf{c}_k^H \mathbf{p}_j|^2 + \mathbf{r}_k^H \mathbf{R}_{\mathbf{q}} \mathbf{r}_k + \sigma_n^2. \tag{3.18}$$

The estimated symbol using the receiver g_k at user k is

$$\begin{aligned} \hat{s}_k &= g_k x_k \\ &= g_k \mathbf{c}_k^H \sum_{j=1}^{K} \mathbf{p}_j s_j + g_k \mathbf{r}_k^H \mathbf{q} + g_k n_k. \end{aligned} \tag{3.19}$$

The MSE is given as

$$\begin{aligned} e_k =& \mathbb{E}\left[\|\hat{s}_k - s_k\|^2 \right] \\ =& |g_k|^2 \left(\sum_{j=1}^{K} |\mathbf{c}_k^H \mathbf{p}_j|^2 + \mathbf{r}_k^H \mathbf{R}_{\mathbf{q}} \mathbf{r}_k + \sigma_n^2 \right) - 2\mathrm{Re}\left\{ g_k \mathbf{c}_k^H \mathbf{p}_k \right\} + 1. \end{aligned} \tag{3.20}$$

The solution to the following unconstrained convex optimization problem yields the MMSE receiver.

$$\begin{aligned} g_k^{\mathrm{MMSE}} &= \arg\min_{g_k} e_k \\ &= \frac{\mathbf{p}_k^H \mathbf{c}_k}{|\mathbf{c}_k^H \mathbf{p}_k|^2 + N_k} \\ &= \frac{\mathbf{p}_k^H \mathbf{c}_k}{\sum_{j=1,}^{K} |\mathbf{c}_k^H \mathbf{p}_j|^2 + \mathbf{r}_k^H \mathbf{R}_{\mathbf{q}} \mathbf{r}_k + \sigma_n^2}. \end{aligned} \tag{3.21}$$

where $\partial e_k / \partial g_k = 0$ is the condition of the optimal MMSE receiver.

The MSE at the output of MMSE receiver is

$$\begin{aligned} e_k^{\mathrm{MMSE}} &= \mathbb{E}\left[(g_k^{\mathrm{MMSE}} x_k - s_k)(g_k^{\mathrm{MMSE}} x_k - s_k)^* \right] \\ &= \left(1 + \frac{|\mathbf{c}_k^H \mathbf{p}_k|^2}{N_k} \right)^{-1} \\ &= 1 - \frac{|\mathbf{c}_k^H \mathbf{p}_k|^2}{\sum_{j=1,}^{K} |\mathbf{c}_k^H \mathbf{p}_j|^2 + \mathbf{r}_k^H \mathbf{R}_{\mathbf{q}} \mathbf{r}_k + \sigma_n^2}. \end{aligned} \tag{3.22}$$

We can formulate another MSE minimization and probing power maximization problem, which is

$$\min_{\mathbf{P},\mathbf{R_q}} \quad \rho \sum_{k=1}^{K} w_k e_k(\mathbf{P},\mathbf{R_q}) - \mathbf{a}_r^H(\varphi_m)\mathbf{R_q}\mathbf{a}_r(\varphi_m) - \mathbf{a}_c^H(\varphi_m)\mathbf{P}\mathbf{P}^H\mathbf{a}_c(\varphi_m) \tag{3.23a}$$

$$\text{s.t.} \quad \text{diag}(\mathbf{R_q}) = \frac{P_r \mathbf{1}^{M_r \times 1}}{M_r}, \tag{3.23b}$$

$$\text{Tr}(\mathbf{P}\mathbf{P}^H) \leq P_c, \tag{3.23c}$$

$$\mathbf{R_q} \succeq 0, \mathbf{R_q} = \mathbf{R_q}^H, \tag{3.23d}$$

According to [40], the problem (3.23) has the same optimal solution of $\{\mathbf{P}, \mathbf{R_q}\}$ as (3.15) for fixed $\mathbf{\Theta}$ as long as

$$w_k = \mu_k (e_k^{\text{MMSE}})^{-1}. \tag{3.24}$$

Problem (3.23) is still non-convex because of the last term. Based on the transformation method in [9], the last term is equal to

$$-\mathbf{a}_c^H(\varphi_m)\mathbf{P}\mathbf{P}^H\mathbf{a}_c(\varphi_m) = \sum_{k=1}^{K} \mathbf{p}_k^H \underbrace{\left(M_c\mathbf{I} - \mathbf{a}_c(\varphi_m)\mathbf{a}_c^H(\varphi_m)\right)}_{\mathbf{Z}(\varphi_m)} \mathbf{p}_k - M_c \times P_c. \tag{3.25}$$

It can be proved that $\mathbf{Z}(\varphi_m)$ is a positive semidefinite matrix, therefore (3.25) is a convex function. The problem (3.23) can be reformulated as

$$\min_{\mathbf{P},\mathbf{R_q}} \quad \rho \sum_{k=1}^{K} w_k e_k(\mathbf{P},\mathbf{R_q}) - \mathbf{a}_r^H(\varphi_m)\mathbf{R_q}\mathbf{a}_r(\varphi_m) + \sum_{k=1}^{K} \mathbf{p}_k^H \mathbf{Z}(\varphi_m)\mathbf{p}_k \tag{3.26a}$$

$$\text{s.t.} \quad \text{diag}(\mathbf{R_q}) = \frac{P_r \mathbf{1}^{M_r \times 1}}{M_r}, \tag{3.26b}$$

$$\text{Tr}(\mathbf{P}\mathbf{P}^H) \leq P_c, \tag{3.26c}$$

$$\mathbf{R_q} \succeq 0, \mathbf{R_q} = \mathbf{R_q}^H. \tag{3.26d}$$

For the fixed $\mathbf{\Theta}$, the maximization of WSR and probing power can be solved by alternating between updating w_k according to (3.24) and solving (3.26). The problem (3.26) is an SDP that the CVX toolbox [41] can effectively solve.

Fractional Programming for Passive Beamforming

For the fixed $\mathbf{P}$ and $\mathbf{R_q}$, the problem (3.15) is simplified to

$$\max_{\mathbf{\Theta}} \quad \sum_{k=1}^{K} \mu_k \log_2(1 + \gamma_k(\mathbf{\Theta})) \tag{3.27a}$$

$$\text{s.t.} \quad \mathbf{\Theta} = \text{diag}(\mathbf{\Theta}_1, \mathbf{\Theta}_2, ..., \mathbf{\Theta}_G), \tag{3.27b}$$

$$\mathbf{\Theta}_g = \mathbf{\Theta}_g^T, \mathbf{\Theta}_g^H \mathbf{\Theta}_g = \mathbf{I}, \forall g. \tag{3.27c}$$

The logarithmic fractional form of WSR and the quadratic equality constraint lead to the non-convexity of problem (3.27). Nevertheless, we show that it can be tackled based on Lagrangian dual transform [25], quadratic transform [24], and scattering-reactance relationship [2].

Applying the Lagrangian dual transform proposed in [25], (3.27) is equivalent to

$$\max_{\boldsymbol{\Theta},\boldsymbol{\alpha}} \quad f(\boldsymbol{\Theta},\boldsymbol{\alpha}) = \sum_{k=1}^{K} \mu_k \log_2(1+\alpha_k) - \sum_{k=1}^{K} \mu_k \alpha_k + \sum_{k=1}^{K} \frac{\mu_k(1+\alpha_k)\gamma_k}{1+\gamma_k} \tag{3.28a}$$

$$\text{s.t.} \quad \boldsymbol{\Theta} = \text{diag}(\boldsymbol{\Theta}_1, \boldsymbol{\Theta}_2, ..., \boldsymbol{\Theta}_G), \tag{3.28b}$$

$$\boldsymbol{\Theta}_g = \boldsymbol{\Theta}_g^T, \boldsymbol{\Theta}_g^H \boldsymbol{\Theta}_g = \mathbf{I}, \forall g. \tag{3.28c}$$

For fixed $\boldsymbol{\Theta}$, (3.28) is an unconstrained convex optimization problem with respect to $\boldsymbol{\alpha} = [\alpha_1, ..., \alpha_K]$ and the optimal $\boldsymbol{\alpha}^\star$ is given as

$$\alpha_k^\star = \gamma_k, \tag{3.29}$$

which is obtained from $\partial f / \partial \alpha_k = 0$.

For the fixed $\boldsymbol{\alpha}$, (3.28) can be simplified to a fractional form

$$\max_{\boldsymbol{\Theta}} \quad \sum_{k=1}^{K} \frac{\mu_k(1+\alpha_k)\gamma_k}{1+\gamma_k} \tag{3.30a}$$

$$\text{s.t.} \quad \boldsymbol{\Theta} = \text{diag}(\boldsymbol{\Theta}_1, \boldsymbol{\Theta}_2, ..., \boldsymbol{\Theta}_G), \tag{3.30b}$$

$$\boldsymbol{\Theta}_g = \boldsymbol{\Theta}_g^T, \boldsymbol{\Theta}_g^H \boldsymbol{\Theta}_g = \mathbf{I}, \forall g, \tag{3.30c}$$

where the logarithm in (3.27) is removed. The problem (3.30) is a sum-of-ratios FP problem. To apply the quadratic transform proposed in [24], we firstly reformulated the objective function of (3.30) by letting $\boldsymbol{\theta} = \text{vec}(\boldsymbol{\Theta}^T)$:

$$\begin{aligned} g(\boldsymbol{\theta}) =& \sum_{k=1}^{K} \frac{\mu_k(1+\alpha_k)\gamma_k}{1+\gamma_k} \\ =& \sum_{k=1}^{K} \frac{\mu_k(1+\alpha_k)|\mathbf{c}_k^H \mathbf{p}_k|^2}{\sum_{j=1}^{K} |\mathbf{c}_k^H \mathbf{p}_j|^2 + \mathbf{r}_k^H \mathbf{R}_\mathbf{q} \mathbf{r}_k + \sigma_n^2} \\ =& \sum_{k=1}^{K} \frac{\mu_k(1+\alpha_k)|(\boldsymbol{\theta}^H \mathbf{A}_k \mathbf{H}_c + \mathbf{d}_{c,k}^H)\mathbf{p}_k|^2}{\sum_{j=1}^{K} |(\boldsymbol{\theta}^H \mathbf{A}_k \mathbf{H}_c + \mathbf{d}_{c,k}^H)\mathbf{p}_j|^2 + (\boldsymbol{\theta}^H \mathbf{A}_k \mathbf{H}_r + \mathbf{d}_{r,k}^H)\mathbf{R}_\mathbf{q}(\mathbf{H}_r^H \mathbf{A}_k^H \boldsymbol{\theta} + \mathbf{d}_{r,k}) + \sigma_n^2}. \end{aligned} \tag{3.31}$$

The matrix $\mathbf{A}_k$ is defined as

$$\mathbf{A}_k = \left[\mathbf{J}^0 \tilde{\mathbf{h}}_k, \mathbf{J}^N \tilde{\mathbf{h}}_k, \mathbf{J}^{2N} \tilde{\mathbf{h}}_k, ..., \mathbf{J}^{(N-1)N} \tilde{\mathbf{h}}_k \right], \tag{3.32}$$

where

$$\tilde{\mathbf{h}}_k = [\mathbf{h}_k^H, \mathbf{0}_{(N-1)N}^T]^T \in \mathbb{C}^{NN \times 1}, \tag{3.33}$$

$$\mathbf{J} = \begin{bmatrix} \mathbf{0}_{NN-1}^T & 0 \\ \mathbf{I}_{NN-1} & \mathbf{0}_{NN-1} \end{bmatrix}. \tag{3.34}$$

The $g(\boldsymbol{\theta})$ can be further simplified to

$$g(\boldsymbol{\theta}) = \sum_{k=1}^{K} \frac{\mu_k(1+\alpha_k)|\boldsymbol{\theta}^H \mathbf{a}_{k,k} + b_{k,k}|^2}{\sum_{j=1}^{K} |\boldsymbol{\theta}^H \mathbf{a}_{j,k} + b_{j,k}|^2 + \boldsymbol{\theta}^H \mathbf{B}_k \boldsymbol{\theta} + 2\mathrm{Re}\left\{\boldsymbol{\theta}^H \mathbf{f}_k\right\} + m_k}, \tag{3.35}$$

where

$$\mathbf{a}_{j,k} = \mathbf{A}_k \mathbf{H}_c \mathbf{p}_j, \tag{3.36}$$
$$b_{j,k} = \mathbf{d}_{c,k}^H \mathbf{p}_j, \tag{3.37}$$
$$\mathbf{B}_k = \mathbf{A}_k \mathbf{H}_r \mathbf{R}_\mathbf{q} \mathbf{H}_r^H \mathbf{A}_k^H, \tag{3.38}$$
$$\mathbf{f}_k = \mathbf{A}_k \mathbf{H}_r \mathbf{R}_\mathbf{q} \mathbf{d}_{r,k}, \tag{3.39}$$
$$m_k = \mathbf{d}_{r,k}^H \mathbf{R}_\mathbf{q} \mathbf{d}_{r.k} + \sigma_n^2. \tag{3.40}$$

As $\mathbf{R}_\mathbf{q}$ is positive semidefinite, it can be written as $\mathbf{R}_\mathbf{q} = \mathbf{R}_d^H \mathbf{R}_d$. Therefore, we have $\mathbf{B}_k = (\mathrm{diag}\{\mathbf{h}_k^H\}\mathbf{H}_r\mathbf{R}_d^H)(\mathrm{diag}\{\mathbf{h}_k^H\}\mathbf{H}_r\mathbf{R}_d^H)^H$, which indicates that $\mathbf{B}_k$ is positive semidefinite.

Applying the quadratic transform of FP proposed in [24], the objective function $g(\boldsymbol{\theta})$ in (3.30) is transformed to a new function $h(\boldsymbol{\theta}, \mathbf{y})$ with $\mathbf{y} = [y_1, ..., y_K]^T$.

$$\begin{aligned} h(\boldsymbol{\theta}, \mathbf{y}) =& \sum_{k=1}^{K} \left(2\mathrm{Re}\left\{y_k^* \sqrt{\mu_k(1+\alpha_k)}\left(\boldsymbol{\theta}^H \mathbf{a}_{k,k} + b_{k,k}\right)\right\}\right) \\ &- \sum_{k=1}^{K} |y_k|^2 \left(\sum_{j=1}^{K} |\boldsymbol{\theta}^H \mathbf{a}_{j,k} + b_{j,k}|^2 + \boldsymbol{\theta}^H \mathbf{B}_k \boldsymbol{\theta} + 2\mathrm{Re}\left\{\boldsymbol{\theta}^H \mathbf{f}_k\right\} + m_k\right). \end{aligned} \tag{3.41}$$

The problem (3.30) is equivalent to

$$\max_{\boldsymbol{\theta}, \mathbf{y}} \quad h(\boldsymbol{\theta}, \mathbf{y}) \tag{3.42a}$$
$$\text{s.t.} \quad \boldsymbol{\theta} = \mathrm{vec}(\boldsymbol{\Theta}^T), \tag{3.42b}$$
$$\boldsymbol{\Theta} = \mathrm{diag}(\boldsymbol{\Theta}_1, \boldsymbol{\Theta}_2, ..., \boldsymbol{\Theta}_G), \tag{3.42c}$$
$$\boldsymbol{\Theta}_g = \boldsymbol{\Theta}_g^T, \boldsymbol{\Theta}_g^H \boldsymbol{\Theta}_g = \mathbf{I}, \forall g, \tag{3.42d}$$
$$\mathbf{y} = [y_1, ..., y_K]^T, y_k \in \mathbb{C}, \forall k. \tag{3.42e}$$

For fixed $\boldsymbol{\theta}$, (3.42) is an unconstrained convex problem with respect to $\mathbf{y}$. By setting $\partial h / \partial y_k$ to zero, we can get the optimal solution:

$$y_k^\star = \frac{\sqrt{\mu_k(1+\alpha_k)}\left(\boldsymbol{\theta}^H \mathbf{a}_{k,k} + b_{k,k}\right)}{\sum_{j=1}^{K} |\boldsymbol{\theta}^H \mathbf{a}_{j,k} + b_{j,k}|^2 + \boldsymbol{\theta}^H \mathbf{B}_k \boldsymbol{\theta} + 2\mathrm{Re}\left\{\boldsymbol{\theta}^H \mathbf{f}_k\right\} + m_k}. \tag{3.43}$$

For fixed $\mathbf{y}$, the term $|\boldsymbol{\theta}^H \mathbf{a}_{j,k} + b_{j,k}|^2$ in $h(\boldsymbol{\theta}, \mathbf{y})$ can be rephrased as

$$\begin{aligned} &|\boldsymbol{\theta}^H \mathbf{a}_{j,k} + b_{j,k}|^2 \\ =&(\boldsymbol{\theta}^H \mathbf{a}_{j,k} + b_{j,k})(\mathbf{a}_{j,k}^H \boldsymbol{\theta} + b_{j,k}^*) \\ =&\boldsymbol{\theta}^H \mathbf{a}_{j,k} \mathbf{a}_{j,k}^H \boldsymbol{\theta} + 2\mathrm{Re}\left\{b_{j,k}^* \boldsymbol{\theta}^H \mathbf{a}_{j,k}\right\} + |b_{j,k}|^2. \end{aligned} \tag{3.44}$$

Substituting this into $h(\boldsymbol{\theta}, \mathbf{y})$ and dropping the constant term, we get a new objective function

$$\tilde{h}(\boldsymbol{\theta}) = -\boldsymbol{\theta}^H \mathbf{U} \boldsymbol{\theta} + 2\mathrm{Re}\left\{\boldsymbol{\theta}^H \mathbf{v}\right\}, \tag{3.45}$$

where

$$\mathbf{U} = \sum_{k=1}^{K} |y_k|^2 \left(\mathbf{B}_k + \sum_{j=1}^{K} \mathbf{a}_{j,k} \mathbf{a}_{j,k}^H \right), \tag{3.46}$$

$$\mathbf{v} = \sum_{k=1}^{K} \left(y_k^* \sqrt{\mu_k (1+\alpha_k)} \mathbf{a}_{k,k} - |y_k|^2 \left(\mathbf{f}_k + \sum_{j=1}^{K} b_{j,k}^* \mathbf{a}_{j,k} \right) \right). \tag{3.47}$$

Thus, the problem (3.42) for fixed $\mathbf{y}$ is simplified to

$$\begin{aligned}
\min_{\boldsymbol{\theta}} \quad & \boldsymbol{\theta}^H \mathbf{U} \boldsymbol{\theta} - 2\mathrm{Re}\left\{\boldsymbol{\theta}^H \mathbf{v}\right\} && \text{(3.48a)} \\
\text{s.t.} \quad & \boldsymbol{\theta} = \mathrm{vec}(\boldsymbol{\Theta}^T) && \text{(3.48b)} \\
& \boldsymbol{\Theta} = \mathrm{diag}(\boldsymbol{\Theta}_1, \boldsymbol{\Theta}_2, ..., \boldsymbol{\Theta}_G), && \text{(3.48c)} \\
& \boldsymbol{\Theta}_g = \boldsymbol{\Theta}_g^T, \boldsymbol{\Theta}_g^H \boldsymbol{\Theta}_g = \mathbf{I}, \forall g. && \text{(3.48d)}
\end{aligned}$$

As $\mathbf{B}_k$ is positive semidefinite, $\mathbf{U}$ is also positive semidefinite. Therefore, the objective functions of (3.48) is convex. However, constrains are still non-convex. In order to tackle this problem, we follow the method proposed in [2], where the relationship between $\boldsymbol{\Theta}_g$ and reactance matrix $\mathbf{Z}_{I,g}$ is exploited, that is

$$\boldsymbol{\Theta}_g = (j\mathbf{Z}_{I,g} + R_0\mathbf{I})^{-1}(j\mathbf{Z}_{I,g} - R_0\mathbf{I}), \forall g, \tag{3.49}$$

$$\mathbf{Z}_{I,g} = \mathbf{Z}_{I,g}^T, \forall g, \tag{3.50}$$

where R_0 refers to the characteristic impedance and is usually set as $R_0 = 50\Omega$. The problem (3.48) can be rewritten as

$$\begin{aligned}
\min_{\boldsymbol{\theta}} \quad & \boldsymbol{\theta}^H \mathbf{U} \boldsymbol{\theta} - 2\mathrm{Re}\left\{\boldsymbol{\theta}^H \mathbf{v}\right\} && \text{(3.51a)} \\
\text{s.t.} \quad & \boldsymbol{\theta} = \mathrm{vec}(\boldsymbol{\Theta}^T) && \text{(3.51b)} \\
& \boldsymbol{\Theta} = \mathrm{diag}(\boldsymbol{\Theta}_1, \boldsymbol{\Theta}_2, ..., \boldsymbol{\Theta}_G), && \text{(3.51c)} \\
& \boldsymbol{\Theta}_g = (j\mathbf{Z}_{I,g} + R_0\mathbf{I})^{-1}(j\mathbf{Z}_{I,g} - R_0\mathbf{I}), \forall g, && \text{(3.51d)} \\
& \mathbf{Z}_{I,g} = \mathbf{Z}_{I,g}^T, \forall g. && \text{(3.51e)}
\end{aligned}$$

The objective of (3.51) is essentially a function of $\mathbf{Z}_{I,g}$. Because $\mathbf{Z}_{I,g}$ can be arbitrary real symmetric matrix, (3.51) is an unconstrained optimization problem that can be addressed by utilising the Quasi-Newton method to optimize the upper triangular part of $\mathbf{Z}_{I,g}$.

In the special case where $G = N$, i.e., single connected network, the passive beamforming matrix $\boldsymbol{\Theta}$ is a diagonal matrix given as

$$\boldsymbol{\Theta} = \mathrm{diag}\{\theta_1, ..., \theta_N\}, \tag{3.52}$$

where $|\theta_i| \leq 1, i = 1, ...N$. Following the same path of deriving (3.51), the following Quadratic Programme (QP) can be obtained.

$$\min_{\breve{\boldsymbol{\theta}}} \quad \breve{\boldsymbol{\theta}}^H \breve{\mathbf{U}} \breve{\boldsymbol{\theta}} - 2\mathrm{Re}\left\{\breve{\boldsymbol{\theta}}^H \breve{\mathbf{v}}\right\} \tag{3.53a}$$

$$\text{s.t.} \quad \breve{\boldsymbol{\theta}} = [\theta_1, ..., \theta_N]^T, \tag{3.53b}$$

$$|\theta_i| \leq 1, \forall i, \tag{3.53c}$$

where

$$\breve{\mathbf{U}} = \sum_{k=1}^{K} |\breve{y}_k|^2 \left(\breve{\mathbf{B}}_k + \sum_{j=1}^{K} \breve{\mathbf{a}}_{j,k} \breve{\mathbf{a}}_{j,k}^H\right), \tag{3.54}$$

$$\breve{\mathbf{v}} = \sum_{k=1}^{K} \left(\breve{y}_k^* \sqrt{\mu_k(1+\alpha_k)} \breve{\mathbf{a}}_{k,k} - |\breve{y}_k|^2 \left(\breve{\mathbf{f}}_k + \sum_{j=1}^{K} b_{j,k}^* \breve{\mathbf{a}}_{j,k}\right)\right), \tag{3.55}$$

$$\breve{y}_k = \frac{\sqrt{\mu_k(1+\alpha_k)} \left(\boldsymbol{\theta}^H \breve{\mathbf{a}}_{k,k} + b_{k,k}\right)}{\sum_{j=1}^{K} |\boldsymbol{\theta}^H \breve{\mathbf{a}}_{j,k} + b_{j,k}|^2 + \boldsymbol{\theta}^H \breve{\mathbf{B}}_k \boldsymbol{\theta} + 2\mathrm{Re}\left\{\boldsymbol{\theta}^H \breve{\mathbf{f}}_k\right\} + m_k}, \tag{3.56}$$

$$\breve{\mathbf{a}}_{j,k} = \mathrm{diag}\{\mathbf{h}_k^H\} \mathbf{H}_c \mathbf{p}_j, \tag{3.57}$$

$$\breve{\mathbf{B}}_k = \mathrm{diag}\{\mathbf{h}_k^H\} \mathbf{H}_r \mathbf{R}_{\mathbf{q}} \mathbf{H}_r^H \mathrm{diag}\{\mathbf{h}_k\}, \tag{3.58}$$

$$\breve{\mathbf{f}}_k = \mathrm{diag}\{\mathbf{h}_k^H\} \mathbf{H}_r \mathbf{R}_{\mathbf{q}} \mathbf{d}_{r,k}. \tag{3.59}$$

$$\tag{3.60}$$

The matrix $\breve{\mathbf{U}}$ can also be proved to be positive semidefinite, therefore (3.53) is a convex QP. Similar to SDP, QP can also be solved by CVX toolbox [41].

Therefore, we propose a WMMSE-FP-based AO algorithm to solve the problem (3.15). The details are shown in Algorithm 1

Algorithm 1 WMMSE-FP-based AO Algorithm for Separated Deployment

Input: $t = 0$, $\mathbf{P}^{[t]}$, $\mathbf{R}_{\mathbf{q}}^{[t]}$, $\boldsymbol{\Theta}^{[t]}$;

1: Calculate $\mathrm{WSR}^{[t]}$ from $\mathbf{P}^{[t]}$, $\mathbf{R}_{\mathbf{q}}^{[t]}$ and $\boldsymbol{\Theta}^{[t]}$;
2: **repeat**
3: $t = t + 1$
4: Calculate $g_k^{[t]}$ by (3.21);
5: Calculate $w_k^{[t]}$ by (3.24);
6: Update active beamforming $\mathbf{P}^{[t]}$ and radar covariance matrix $\mathbf{R}_{\mathbf{q}}^{[t]}$ by solving (3.26);
7: Calculate $\alpha_k^{[t]}$ by (3.29);
8: Calculate $y_k^{[t]}$ by (3.43) for group/fully connected RIS or $\breve{y}_k^{[t]}$ by (3.56) for single connected RIS;
9: Update $\boldsymbol{\Theta}^{[t]}$ by solving (3.51) for group/fully connected RIS or (3.53) for single connected RIS;
10: Calculate $\mathrm{WSR}^{[t]}$ from $\mathbf{P}^{[t]}$, $\mathbf{R}_{\mathbf{q}}^{[t]}$ and $\boldsymbol{\Theta}^{[t]}$;
11: **until** $\left|\mathrm{WSR}^{[t-1]} - \mathrm{WSR}^{[t]}\right| \leq \epsilon$.

3.3.2 Algorithm for Shared Deployment

For fixed $\mathbf{\Theta}$, we firstly follow the same path in Section 3.3.1 and reformulate (3.16) using WMMSE as

$$\min_{\check{\mathbf{p}}_1,...,\check{\mathbf{p}}_K} \quad \rho\sum_{k=1}^{K}\check{w}_k\check{e}_k(\check{\mathbf{p}}_1,...,\check{\mathbf{p}}_K)+\sum_{k=1}^{K}\check{\mathbf{p}}_k^H\mathbf{Z}(\varphi_m)\check{\mathbf{p}}_k \tag{3.61a}$$

$$\text{s.t.} \quad \text{diag}\left(\sum_{j=1}^{K}\check{\mathbf{p}}_j\check{\mathbf{p}}_j^H\right)=\frac{P}{M}\mathbf{1}^{M\times 1}, \tag{3.61b}$$

where

$$\check{e}_k=|\check{g}_k|^2\left(\sum_{j=1}^{K}|\check{\mathbf{c}}_k^H\check{\mathbf{p}}_j|^2+\sigma_n^2\right)-2\text{Re}\{g_k\check{\mathbf{c}}_k^H\check{\mathbf{p}}_k\}+1, \tag{3.62}$$

$$\check{g}_k^{\text{MMSE}}=\frac{\check{\mathbf{p}}_k^H\check{\mathbf{c}}_k}{\sum_{j=1}^{K}|\check{\mathbf{c}}_k^H\check{\mathbf{p}}_j|^2+\sigma_n^2}, \tag{3.63}$$

$$\check{e}_k^{\text{MMSE}}=1-\frac{|\check{\mathbf{c}}_k^H\check{\mathbf{p}}_k|^2}{\sum_{j=1}^{K}|\check{\mathbf{c}}_k^H\check{\mathbf{p}}_j|^2+\sigma_n^2}, \tag{3.64}$$

$$\check{w}_k=\mu_k(\check{e}^{\text{MMSE}})^{-1}, \tag{3.65}$$

$$\mathbf{Z}(\varphi_m)=\Big(M\mathbf{I}-\mathbf{a}(\varphi_m)\mathbf{a}^H(\varphi_m)\Big). \tag{3.66}$$

The non-convexity of this problem is from the quadratic equality constraint. In [9], the authors proposed an MM algorithm to address it. But the MM is an iterative algorithm, which leads to high complexity when it is nested in an outer iterative loop. Thus, we propose a new low complexity algorithm based on SDR, which is capable of solving this problem in one step. Observing that this problem is an inhomogeneous QCQP, we firstly homogenize this problem.

The $\check{e}_k$ can be rewritten as

$$\begin{aligned}\check{e}_k&=|\check{g}_k|^2\left(\sum_{j=1}^{K}|\check{\mathbf{c}}_k^H\check{\mathbf{p}}_j|^2+\sigma_n^2\right)-2\text{Re}\{\check{g}_k\check{\mathbf{c}}_k^H\check{\mathbf{p}}_k\}+1\\&=|\check{g}_k|^2\sum_{j=1}^{K}\check{\mathbf{p}}_j^H\check{\mathbf{c}}_k\check{\mathbf{c}}_k^H\check{\mathbf{p}}_j+|\check{g}_k|^2\sigma_n^2-\check{g}_k\check{\mathbf{c}}_k^H\check{\mathbf{p}}_k-\check{g}_k^*\check{\mathbf{p}}_k^H\check{\mathbf{c}}_k+1\end{aligned} \tag{3.67}$$

Omit the constants and reformulate it as

$$\begin{aligned}\hat{e}_k&=|\check{g}_k|^2\sum_{j=1}^{K}\check{\mathbf{p}}_j^H\check{\mathbf{c}}_k\check{\mathbf{c}}_k^H\check{\mathbf{p}}_j-\check{g}_k\check{\mathbf{c}}_k^H\check{\mathbf{p}}_k-\check{g}_k^*\check{\mathbf{p}}_k^H\check{\mathbf{c}}_k\\&=|\check{g}_k|^2\sum_{j=1,j\neq k}^{K}\check{\mathbf{p}}_j^H\check{\mathbf{c}}_k\check{\mathbf{c}}_k^H\check{\mathbf{p}}_j+|\check{g}_k|^2\check{\mathbf{p}}_k^H\check{\mathbf{c}}_k\check{\mathbf{c}}_k^H\check{\mathbf{p}}_k-\check{g}_k\check{\mathbf{c}}_k^H\check{\mathbf{p}}_k-\check{g}_k^*\check{\mathbf{p}}_k^H\check{\mathbf{c}}_k\\&=\sum_{j=1,j\neq k}^{K}\begin{bmatrix}\hat{\mathbf{p}}_j^H & t_j^*\end{bmatrix}\begin{bmatrix}|\check{g}_k|^2\check{\mathbf{c}}_k\check{\mathbf{c}}_k^H & \mathbf{0}\\ \mathbf{0}^T & 0\end{bmatrix}\begin{bmatrix}\hat{\mathbf{p}}_j\\ t_j\end{bmatrix}+\begin{bmatrix}\hat{\mathbf{p}}_k^H & t_k^*\end{bmatrix}\begin{bmatrix}|\check{g}_k|^2\check{\mathbf{c}}_k\check{\mathbf{c}}_k^H & -\check{g}_k^*\check{\mathbf{c}}_k\\ -\check{g}_k\check{\mathbf{c}}_k^H & 0\end{bmatrix}\begin{bmatrix}\hat{\mathbf{p}}_k\\ t_k\end{bmatrix}\end{aligned} \tag{3.68}$$

where $|t_j|^2 = 1$ and $\hat{\mathbf{p}}_j = t_j \check{\mathbf{p}}_j$.

Similarly, we have

$$\check{\mathbf{p}}_k^H \mathbf{Z}(\varphi_m) \check{\mathbf{p}}_k = \begin{bmatrix} \hat{\mathbf{p}}_k^H & t_k^* \end{bmatrix} \begin{bmatrix} \mathbf{Z}(\varphi_m) & \mathbf{0} \\ \mathbf{0}^T & 0 \end{bmatrix} \begin{bmatrix} \hat{\mathbf{p}}_k \\ t_k \end{bmatrix} \tag{3.69}$$

The constraint can also be rewritten as

$$\begin{aligned} &\operatorname{diag}\left(\sum_{j=1}^{K} \check{\mathbf{p}}_j \check{\mathbf{p}}_j^H \right) = \frac{P}{M} \mathbf{1}^{M \times 1} \\ &\Longrightarrow \operatorname{diag}\left(\sum_{j=1}^{K} \begin{bmatrix} \hat{\mathbf{p}}_j \\ t_j \end{bmatrix} \begin{bmatrix} \hat{\mathbf{p}}_j^H & t_j^* \end{bmatrix} \right) = \begin{bmatrix} \frac{P}{M} \mathbf{1}^{M \times 1} \\ \sum_{j=1}^{K} |t_j|^2 \end{bmatrix} = \begin{bmatrix} \frac{P}{M} \mathbf{1}^{M \times 1} \\ K \end{bmatrix} \end{aligned} \tag{3.70}$$

Therefore, we can obtain a new homogenous QCQP optimization problem

$$\min_{\tilde{\mathbf{p}}_1, \cdots \tilde{\mathbf{p}}_K} \quad \sum_{k=1}^{K} \left(\hat{w}_k \sum_{j=1, j \neq k}^{K} \tilde{\mathbf{p}}_j^H \mathbf{C}_{k,1} \tilde{\mathbf{p}}_j + \hat{w}_k \tilde{\mathbf{p}}_k^H \mathbf{C}_{k,2} \tilde{\mathbf{p}}_k + \tilde{\mathbf{p}}_k^H \hat{\mathbf{Z}}(\varphi_m) \tilde{\mathbf{p}}_k \right) \tag{3.71a}$$

$$\text{s.t.} \quad \operatorname{diag}\left(\sum_{k=1}^{K} \tilde{\mathbf{p}}_k \tilde{\mathbf{p}}_k^H \right) = \begin{bmatrix} \frac{P}{M} \mathbf{1}^{M \times 1} \\ K \end{bmatrix}, \tag{3.71b}$$

$$|[\tilde{\mathbf{p}}_k]_{M+1}|^2 = 1, k = 1, ..., K, \tag{3.71c}$$

where

$$\hat{w}_k = \rho \check{w}_k, \tag{3.72}$$

$$\tilde{\mathbf{p}}_k = \begin{bmatrix} \hat{\mathbf{p}}_k \\ t_k \end{bmatrix}, \tag{3.73}$$

$$\mathbf{C}_{k,1} = \begin{bmatrix} |\check{g}_k|^2 \check{\mathbf{c}}_k \check{\mathbf{c}}_k^H & \mathbf{0} \\ \mathbf{0}^T & 0 \end{bmatrix}, \tag{3.74}$$

$$\mathbf{C}_{k,2} = \begin{bmatrix} |\check{g}_k|^2 \check{\mathbf{c}}_k \check{\mathbf{c}}_k^H & -\check{g}_k^* \check{\mathbf{c}}_k \\ -\check{g}_k \check{\mathbf{c}}_k^H & 0 \end{bmatrix}, \tag{3.75}$$

$$\hat{\mathbf{Z}}(\varphi_m) = \begin{bmatrix} \mathbf{Z}(\varphi_m) & \mathbf{0} \\ \mathbf{0}^T & 0 \end{bmatrix}, \tag{3.76}$$

and $[\tilde{\mathbf{p}}_k]_{M+1}$ denotes the $(M+1)$-th element of $\tilde{\mathbf{p}}_k$.

Letting $\mathbf{T}_k = \tilde{\mathbf{p}}_k \tilde{\mathbf{p}}_k^H$ and omitting the rank-one constraint, we obtain the SDR of the homogenous QCQP problem:

$$\min_{\mathbf{T}_1, \ldots, \mathbf{T}_k} \quad \sum_{k=1}^{K} \left(\hat{w}_k \sum_{j=1, j \neq k}^{K} \operatorname{Tr}(\mathbf{C}_{k,1} \mathbf{T}_j) + \hat{w}_k \operatorname{Tr}(\mathbf{C}_{k,2} \mathbf{T}_k) + \operatorname{Tr}(\hat{\mathbf{Z}}(\varphi_m) \mathbf{T}_k) \right) \tag{3.77a}$$

$$\text{s.t.} \quad \operatorname{diag}\left(\sum_{k=1}^{K} \mathbf{T}_k \right) = \begin{bmatrix} \frac{P}{M} \mathbf{1}^{M \times 1} \\ K \end{bmatrix}, \tag{3.77b}$$

$$[\mathbf{T}_k]_{M+1, M+1} = 1, k = 1, ..., K, \tag{3.77c}$$

$$\mathbf{T}_k \succeq 0, \mathbf{T}_k = \mathbf{T}_k^H, k = 1, ..., K, \tag{3.77d}$$

where $[\mathbf{T}_k]_{M+1,M+1}$ denotes the entry at $(M+1)$-th row and $(M+1)$-th column.

CVX toolbox can easily handle this problem. After finding the optimal $\mathbf{T}_k^\star$, we can use the eigenvalue decomposition or Gaussian randomization method [33] to approximate the solution $\tilde{\mathbf{p}}_k^\star$ to the QCQP (3.71). The optimal solution $\check{\mathbf{p}}_k^\star$ to (3.61) can be obtained by

$$\check{\mathbf{p}}_k^\star = \frac{1}{t_k^\star}\hat{\mathbf{p}}_k^\star, \tag{3.78}$$

where $t_k^\star = [\tilde{\mathbf{p}}_k^\star]_{M+1}$ and $\hat{\mathbf{p}}_k^\star = [\tilde{\mathbf{p}}_k^\star]_{1:M}$.

For fixed $\check{\mathbf{p}}_k, k = 1, ...K$, the optimization problem of $\boldsymbol{\Theta}$ is similar as that in Section 3.3.1 and the following optimization problem for group connected RIS can be obtained:

$$\begin{aligned}
\min_{\boldsymbol{\theta}} \quad & \boldsymbol{\theta}^H \check{\mathbf{U}} \boldsymbol{\theta} - 2\mathrm{Re}\left\{\boldsymbol{\theta}^H \check{\mathbf{v}}\right\} && \text{(3.79a)}\\
\text{s.t.} \quad & \boldsymbol{\theta} = \mathrm{vec}(\boldsymbol{\Theta}^T), && \text{(3.79b)}\\
& \boldsymbol{\Theta} = \mathrm{diag}(\boldsymbol{\Theta}_1, \boldsymbol{\Theta}_2, ..., \boldsymbol{\Theta}_G), && \text{(3.79c)}\\
& \boldsymbol{\Theta}_g = (j\mathbf{Z}_{I,g} + R_0\mathbf{I})^{-1}(j\mathbf{Z}_{I,g} - R_0\mathbf{I}), \forall g, && \text{(3.79d)}\\
& \mathbf{Z}_{I,g} = \mathbf{Z}_{I,g}^T, \forall g, && \text{(3.79e)}
\end{aligned}$$

where

$$\check{\mathbf{U}} = \sum_{k=1}^{K} |\check{y}_k|^2 \sum_{j=1}^{K} \check{\mathbf{a}}_{j,k}\check{\mathbf{a}}_{j,k}^H, \tag{3.80}$$

$$\check{\mathbf{v}} = \sum_{k=1}^{K} \left(\check{y}_k^* \sqrt{\mu_k(1+\check{\alpha}_k)}\check{\mathbf{a}}_{k,k} - |\check{y}_k|^2 \sum_{j=1}^{K} \check{b}_{j,k}^* \check{\mathbf{a}}_{j,k} \right), \tag{3.81}$$

$$\check{y}_k = \frac{\sqrt{\mu_k(1+\check{\alpha}_k)}\left(\boldsymbol{\theta}^H\check{\mathbf{a}}_{k,k} + \check{b}_{k,k}\right)}{\sum_{j=1}^{K}|\boldsymbol{\theta}^H\check{\mathbf{a}}_{j,k} + \check{b}_{j,k}|^2 + \sigma_n^2}, \tag{3.82}$$

$$\check{\mathbf{a}}_{j,k} = \mathbf{A}_k\mathbf{H}\check{\mathbf{p}}_j, \tag{3.83}$$

$$\check{b}_{j,k} = \mathbf{d}_k^H\check{\mathbf{p}}_j, \tag{3.84}$$

$$\check{\alpha}_k = \check{\gamma}_k. \tag{3.85}$$

The simplified optimization problem for single connected RIS is

$$\begin{aligned}
\min_{\check{\boldsymbol{\theta}}} \quad & \check{\boldsymbol{\theta}}^H \bar{\mathbf{U}} \check{\boldsymbol{\theta}} - 2\mathrm{Re}\left\{\check{\boldsymbol{\theta}}^H \bar{\mathbf{v}}\right\} && \text{(3.86a)}\\
\text{s.t.} \quad & \check{\boldsymbol{\theta}} = [\theta_1, ..., \theta_N]^T, && \text{(3.86b)}\\
& |\theta_i| \leq 1, \forall i, && \text{(3.86c)}
\end{aligned}$$

where

$$\bar{\mathbf{U}} = \sum_{k=1}^{K} |\bar{y}_k|^2 \sum_{j=1}^{K} \bar{\mathbf{a}}_{j,k} \bar{\mathbf{a}}_{j,k}^H, \tag{3.87}$$

$$\bar{\mathbf{v}} = \sum_{k=1}^{K} \left(\bar{y}_k^* \sqrt{\mu_k(1+\alpha_k)} \bar{\mathbf{a}}_{k,k} - |\bar{y}_k|^2 \sum_{j=1}^{K} \check{b}_{j,k}^* \bar{\mathbf{a}}_{j,k} \right), \tag{3.88}$$

$$\bar{y}_k = \frac{\sqrt{\mu_k(1+\check{\alpha}_k)} \left(\boldsymbol{\theta}^H \bar{\mathbf{a}}_{k,k} + \check{b}_{k,k} \right)}{\sum_{j=1}^{K} |\boldsymbol{\theta}^H \bar{\mathbf{a}}_{j,k} + \check{b}_{j,k}|^2 + \sigma_n^2}, \tag{3.89}$$

$$\bar{\mathbf{a}}_{j,k} = \text{diag}\{\mathbf{h}_k^H\} \mathbf{H} \check{\mathbf{p}}_j. \tag{3.90}$$

Similarly, (3.79) and (3.86) can be respectively solved using Quasi-Newton method in MATLAB and CVX toolbox.

Thus, we propose another WMMSE-FP-based AO algorithm summarized as Algorithm 2 to solve the problem (3.16).

Algorithm 2 WMMSE-FP-based AO Algorithm for Shared Deployment

Input: $t = 0$, $\check{\mathbf{p}}_1^{[t]}, ..., \check{\mathbf{p}}_K^{[t]}$, $\boldsymbol{\Theta}^{[t]}$;

1: Calculate $\text{WSR}^{[t]}$ from $\check{\mathbf{p}}_1^{[t]}, ..., \check{\mathbf{p}}_K^{[t]}$ and $\boldsymbol{\Theta}^{[t]}$;
2: **repeat**
3: $t = t + 1$;
4: Calculate $g_k^{[t]}$ by (3.63);
5: Calculate $w_k^{[t]}$ by (3.65);
6: Calculate $\mathbf{T}_k^\star$ from (3.77) and approximate $\tilde{\mathbf{p}}_k^\star$ using eigenvalue decomposition or Gaussian randomization;
7: Update $\check{\mathbf{p}}_1^{[t]}, ..., \check{\mathbf{p}}_K^{[t]}$ by (3.78);
8: Calculate $\alpha_k^{[t]}$ by (3.85);
9: Calculate $y_k^{[t]}$ by (3.82) for group/fully connected RIS or $\check{y}_k^{[t]}$ by (3.89) for single connected RIS;
10: update $\boldsymbol{\Theta}^{[t]}$ by solving (3.79) for group/fully connected RIS or (3.86) for single connected RIS;
11: Calculate $\text{WSR}^{[t]}$ from $\check{\mathbf{p}}_1^{[t]}, ..., \check{\mathbf{p}}_K^{[t]}$ and $\boldsymbol{\Theta}^{[t]}$;
12: **until** $\left| \text{WSR}^{[t-1]} - \text{WSR}^{[t]} \right| \leq \epsilon$.

Chapter 4

Performance Evaluation

As [8], we consider a RIS-aided femtocell network shown in Fig.4.1. The BS is equipped with a ULA array with $M = 16$ antennas, and the RIS is equipped with $N = 20$ linearly-deployed reflecting elements. The system serves $K = 4$ downlink users with a power budget of $P = 20$dBm and noise power of -117dBm. The direction of the radar target is 0° from BS.

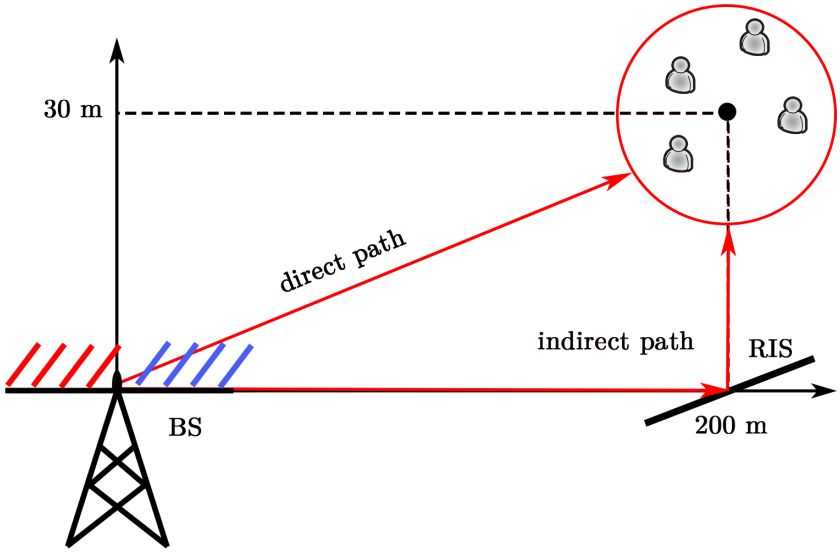

Figure 4.1: The simulated RIS-aided femtocell network

In separated deployment, the resources are equally divided and allocated to radar and communication functions, i.e., $M_c = M_r = M/2$ and $P_c = P_r = P/2$. We assume that the BS-RIS and RIS-user channel follows the Rician fading and the BS-user channel experiences the Rayleigh fading. Thus, the channels $\mathbf{H}_c$, $\mathbf{H}_r$ and

$\mathbf{h}_k$ are modeled as

$$\mathbf{H}_c = \sqrt{L_{BR}}\left(\sqrt{\frac{\varepsilon}{\varepsilon+1}}\mathbf{a}_{\mathrm{RIS}}(\vartheta)\mathbf{a}_c^H(\varphi) + \sqrt{\frac{1}{\varepsilon+1}}\check{\mathbf{H}}_c\right) \tag{4.1}$$

$$\mathbf{H}_r = \sqrt{L_{BR}}\left(\sqrt{\frac{\varepsilon}{\varepsilon+1}}\mathbf{a}_{\mathrm{RIS}}(\vartheta)\mathbf{a}_r^H(\varphi) + \sqrt{\frac{1}{\varepsilon+1}}\check{\mathbf{H}}_r\right) \tag{4.2}$$

$$\mathbf{h}_k = \sqrt{L_{RU}}\left(\sqrt{\frac{\varepsilon}{\varepsilon+1}}\mathbf{a}_{\mathrm{RIS}}(\varsigma_k) + \sqrt{\frac{1}{\varepsilon+1}}\check{\mathbf{h}}_k\right) \tag{4.3}$$

where L_{BR} and L_{RU} are the path loss, ε is the Rician factor and $(\check{\mathbf{H}}_c, \check{\mathbf{H}}_r, \check{\mathbf{h}}_k)$ are NLOS components that follow Rayleigh fading. The BS-user channels $\mathbf{d}_{r,k}$ and $\mathbf{d}_{c,k}$ are assumed to follow Rayleigh fading. In the baseline, only the direct channels $\mathbf{d}_{r,k}$ and $\mathbf{d}_{c,k}$ are considered.

In shared deployment, the channel $\mathbf{H}$ is similarly formulated as

$$\mathbf{H} = \sqrt{L_{BR}}\left(\sqrt{\frac{\varepsilon}{\varepsilon+1}}\mathbf{a}_{\mathrm{RIS}}(\vartheta)\mathbf{a}^H(\varphi) + \sqrt{\frac{1}{\varepsilon+1}}\check{\mathbf{H}}\right) \tag{4.4}$$

Table 4.1 shows the detailed simulation parameters which is similar to [8]. In particular, the path loss model is defined based on 3GPP propagation environment [42].

Table 4.1: Simulation parameters

	Parameter	Value
Transceiver	BS Location	$(0\text{m}, 0\text{m})$
	RIS Location	$(200\text{m}, 0\text{m})$
	User Location	within 10m from $(30\text{m}, 200\text{m})$
	Target Direction	0° from BS
	Number of Users	$K = 4$
	Antennas at BS	$M = 16$
	Reflecting Elements	$N = 20$
	Transmit power	$P = 20\text{dBm}$
	Noise power	$\sigma_n^2 = -117\text{dBm}$
Channel	Indirect Path Loss	$35.6 + 22.0\log_{10}(d)$ dB
	Direct Path Loss	$32.6 + 36.7\log_{10}(d)$ dB

4.1 Convergence

The convergence of the proposed algorithms is demonstrated in this part. Figure 4.2 shows that the proposed algorithms for both separated and shared deployments can converge in 10 iterations, which indicates the low complexity of the proposed algorithms.

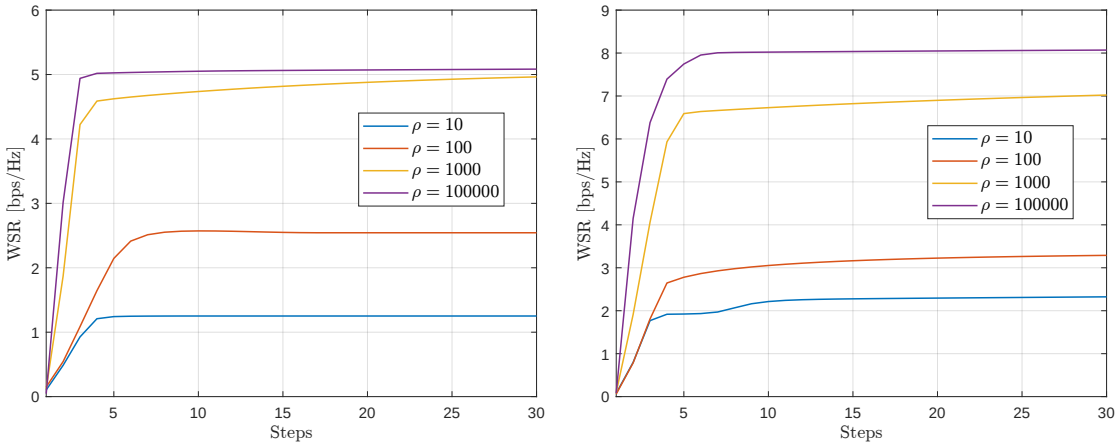

(a) Algorithm for separated deployment

(b) Algorithm for shared deployment

Figure 4.2: Convergence of proposed algorithms

Note that in Figure 4.2(b), the eigenvalue decomposition in used to approximate $\tilde{\mathbf{p}}_k^\star$ in SDR. In Figure 4.3, we compare the eigenvalue decomposition and Gaussian randomization in Algorithm 2 when $\rho = 100000$. It can be observed that the algorithm cannot converge when the Gaussian randomization is applied. The reason is that the $\tilde{\mathbf{T}}_k^\star$ calculated by CVX toolbox in practice is almost rank-one, i.e., the eigenvalues except the largest one are almost zero. In this case, the Gaussian randomization cannot guarantee a good rank-one approximation.

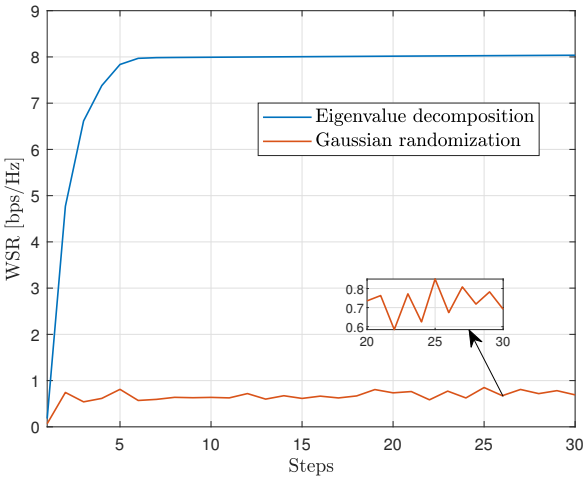

Figure 4.3: Comparison of eigenvalue decomposition and Gaussian randomization

4.2 Transmission Beampattern Comparison

In this section, we demonstrate the beampatterns obtained from Algorithm 1 and 2 and the baselines in both LOS-dominated Rician channel and Rayleigh channel.

Figure 4.4 compares the averaged beampattern from Monte-Carlo simulation when BS-RIS and RIS-user channels follow Rayleigh fading ($\varepsilon = 0$). One can visualize from Figure 4.4(a) and 4.4(c) that both single connected and fully connected

RIS make tiny improvement to the beampattern compared with baseline when the WSR is small. However, as shown in Figure 4.4(b) and 4.4(d), when WSR increases to a large value, i.e., 5.4bps/Hz and 7.9bps/Hz, fully connected RIS achieves the largest probing power at target. The gains achieved by fully connected RIS in separated deployment over single connected RIS and baseline are 2.2dB and 4.7dB, respectively. The counterparts in shared deployment are 2.7dB and 4.8dB.

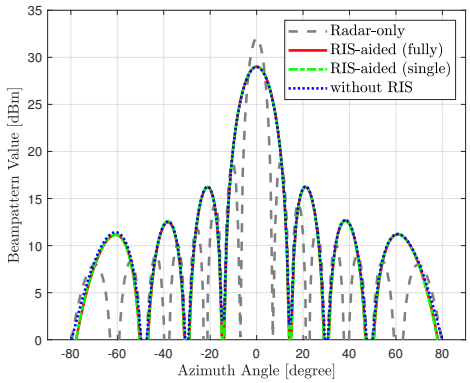

(a) Separated deployment: WSR = 1.0bps/Hz

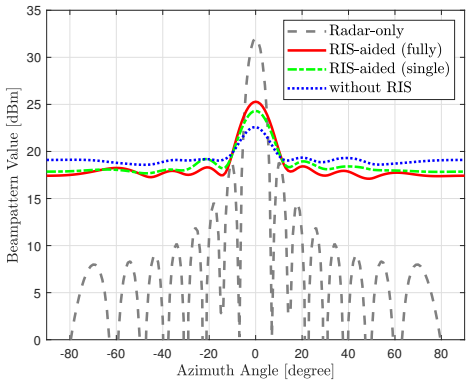

(b) Separated deployment: WSR = 5.4bps/Hz

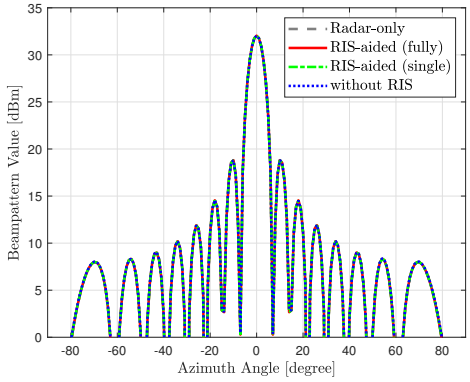

(c) Shared deployment: WSR = 1.8bps/Hz

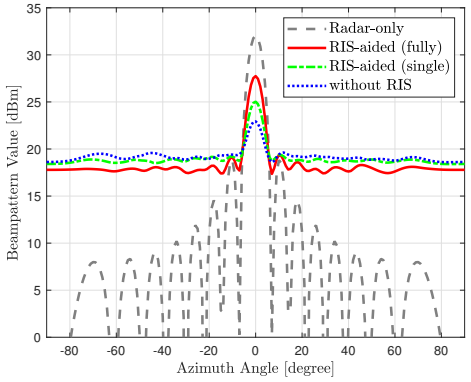

(d) Shared deployment: WSR = 7.9bps/Hz

Figure 4.4: Beampattern comparison in Rayleigh channel ($\varepsilon = 0$)

Figure 4.5 compares the averaged beampattern when the BS-RIS and RIS-user channels are LOS-dominated Rician channel ($\varepsilon = 1000$). We can see that in both separated and shared deployment the fully connected RIS does not outperform the single connected RIS significantly in terms of probing power no matter the WSR is large or small. Therefore, the fully connected only shows advantages when the BS-RIS and RIS-user channels follow Rayleigh fading. The scaling law in [2] indicates that the fully connected and single connected RIS achieves the same received power at users in LOS channel because the model of LOS channel leads to the same optimal $\boldsymbol{\Theta}$. This scaling law can also explain the results in Figure 4.5: the model of LOS channel also leads to the same optimal $\boldsymbol{\Theta}$ in terms of WSR, so that the WSR is the same when the probing power at target is the same.

Figure 4.6 shows the effect of the number of reflecting elements in LOS-dominated Rician channel. As the fully connected and single connected RIS perform the same in LOS channel, only single connected RIS is considered in Figure 4.6. We can see

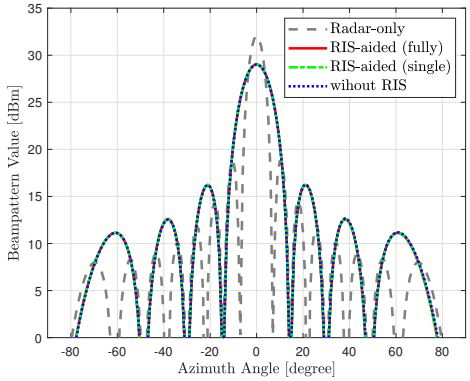

(a) Separated deployment: WSR = 1.0bps/Hz

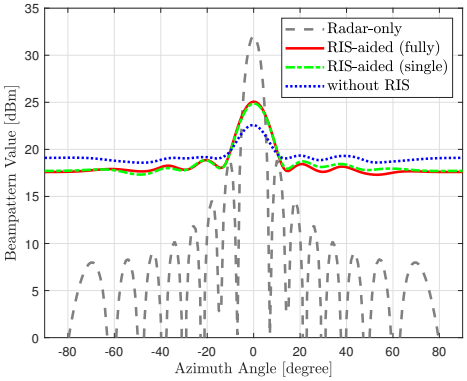

(b) Separated deployment: WSR = 5.4bps/Hz

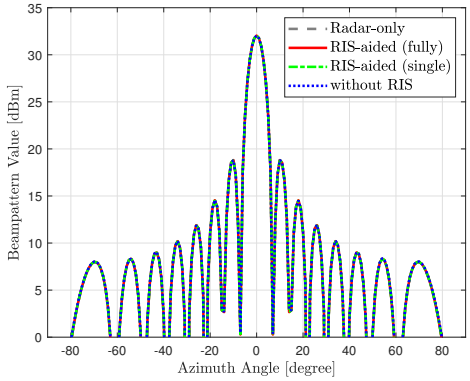

(c) Shared deployment: WSR = 1.8bps/Hz

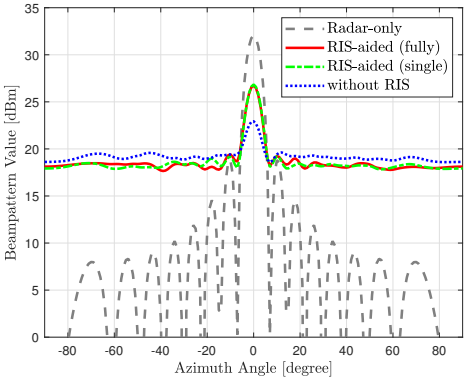

(d) Shared deployment: WSR = 7.9bps/Hz

Figure 4.5: Beampattern comparison in LOS-dominated Rician channel ($\varepsilon = 1000$)

that the better beampattern and higher probing power at target are achieved as the growth of element amounts. Nevertheless, the improvement is not to infinity but asymptotically reaches an upper bound. For example, in shared deployment, the probing power at target increases by 4.9dB as the reflecting element increases from 0 to 20, while the gains are reduced to 1.2dB and 0.2dB when the amount changes from 20 to 60 and from 60 to 100, respectively.

Figure 4.7 compares the beampattern of separated and shared deployments. It displays that the mainlobe of beampattern in shared deployment is much more narrow than that in separated deployment, which is more directional. With the help of RIS, the probing power at target in shared deployment is only 0.13dB lower than the Radar-only system when there are 100 reflecting elements.

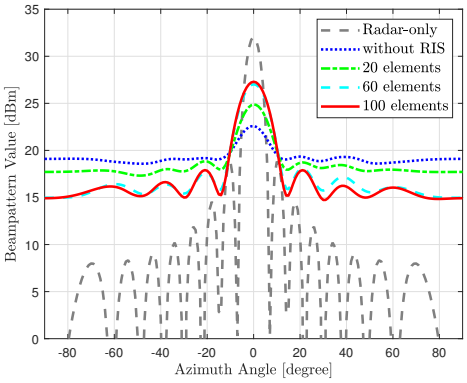

(a) Separated deployment: WSR = 5.4bps/Hz

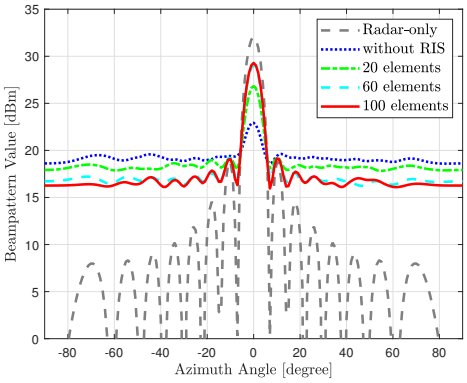

(b) Shared deployment: WSR = 7.9bps/Hz

Figure 4.6: Effect of the number of reflecting elements on beampattern in LOS-dominated Rician channel

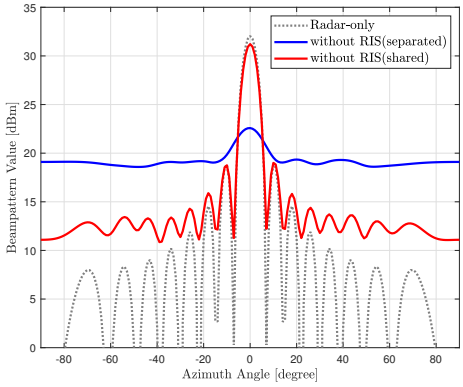

(a) without RIS, WSR = 5.4bps/Hz

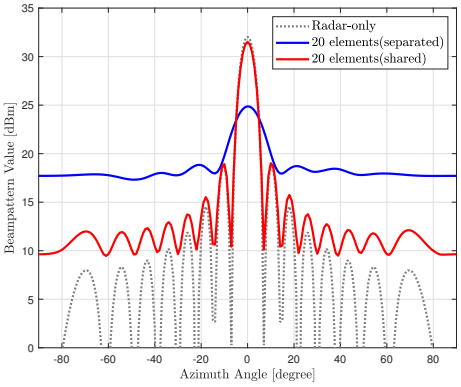

(b) 20 elements, WSR = 5.4bps/Hz

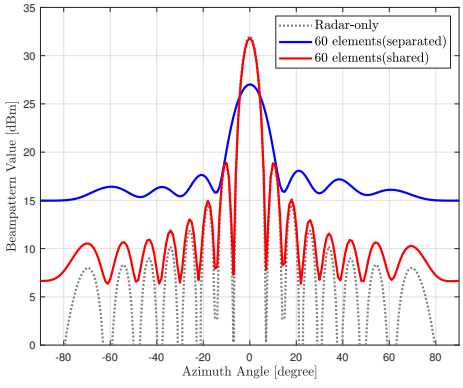

(c) 60 elements, WSR = 5.4bps/Hz

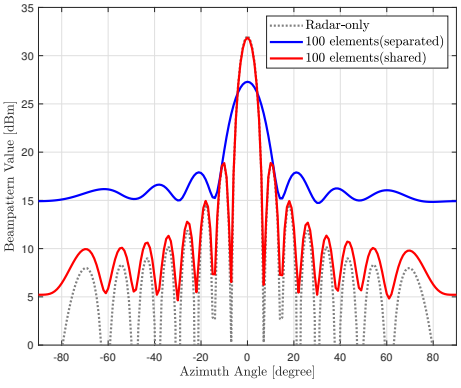

(d) 100 elements, WSR = 5.4bps/Hz

Figure 4.7: Beampattern comparison of separated and share deployment in LOS-dominated Rician channel

4.3 Tradeoff Comparison

As problem (3.15) and (3.16) are multi-objective optimization problems, we can obtain the Pareto optimal front by varying the regularization parameter ρ, which is capable of revealing the tradeoff relationship between different objectives, i.e., probing power at target and WSR. Figure 4.8 shows the Pareto optimal fronts of the RIS-aided and normal DFRC systems.

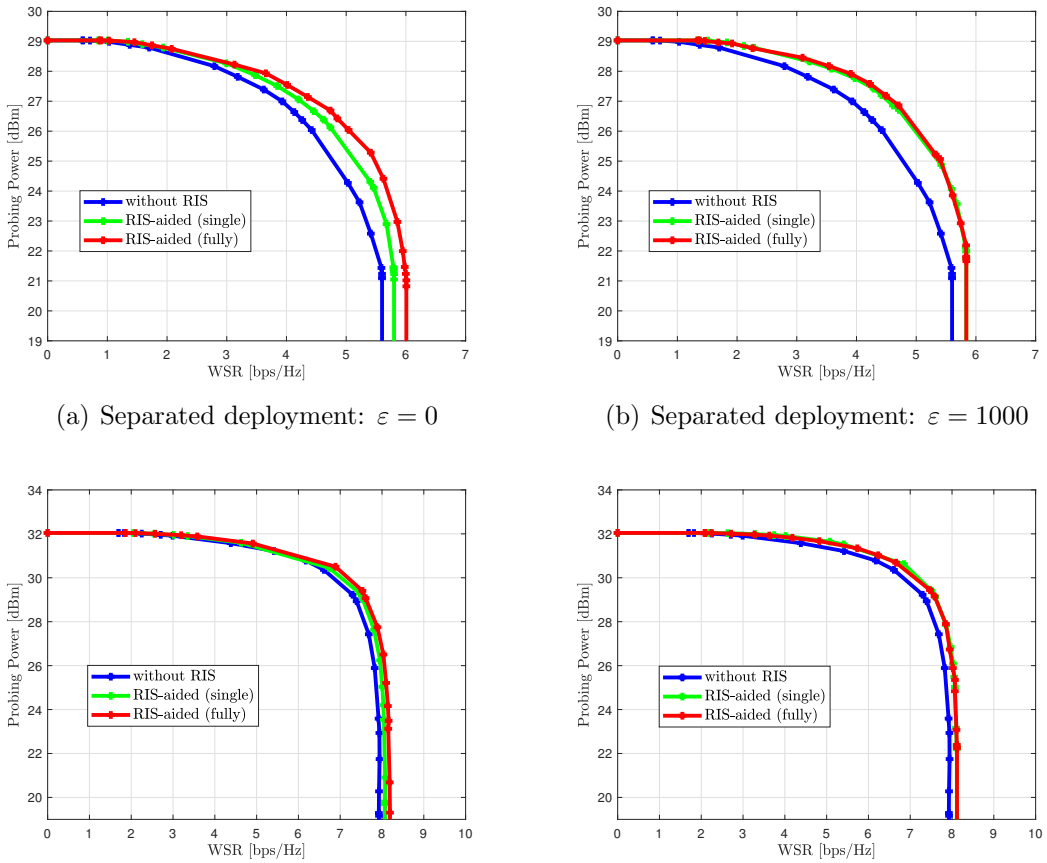

(a) Separated deployment: $\varepsilon = 0$

(b) Separated deployment: $\varepsilon = 1000$

(c) Shared deployment: $\varepsilon = 0$

(d) Shared deployment: $\varepsilon = 1000$

Figure 4.8: Tradeoff between probing power at target and WSR

In Figure 4.8(a), it is obvious that we must decrease the probing power to increase the WSR and vice versa, which is a tradeoff. It is also clear that the RIS shows advantages compared with DFRC without RIS.

For separated deployment, when the BS-RIS and RIS-user channels are Rayleigh channel (shown in Figure 4.8(a)), the fully connected RIS performs best, which has a 6.0bps/Hz upper bound of WSR. The single connected RIS is capable of achieving 5.8bps/Hz upper bound of WSR, which is 0.20bps/Hz higher than that achieved in the baseline. Figure 4.8(b) shows that case where the channel is LOS dominated. One can visualize that the fully connected and single connected RIS has the same performance, which further validates the result in Section 4.2.

Figure 4.8(c) and 4.8(d) show that the fully connected RIS only outperforms single connected RIS in Rayleigh channel for shared deployment, which is the same as

separated deployment. However, the gain from RIS is smaller than that in separated deployment, which is 0.15bps/Hz and 0.27bps/Hz for single connected and fully connected RIS in Rayleigh channel, respectively.

Although the RIS can increase the WSR upper bound, the probing power upper bounds are all 29dBm in separated deployment and 32dBm in shared deployment. The reason is that the probing power upper bound is determined by the capability of BS, which is the same when there is RIS or not. There is a 3dB gain of probing power upper bound for shared deployment over separated deployment.

We now evaluate the performance of DFRC aided by single connected RIS in LOS-dominated Rician channel with various numbers of reflecting elements. In Figure 4.9, we can see that the DFRC systems have the larger achievable region and higher WSR upper bounds as the increase of reflecting elements. The RIS with 100 elements is capable of improving the WSR by 0.82bps/Hz in separated deployment and 0.58bps/Hz in shared deployment.

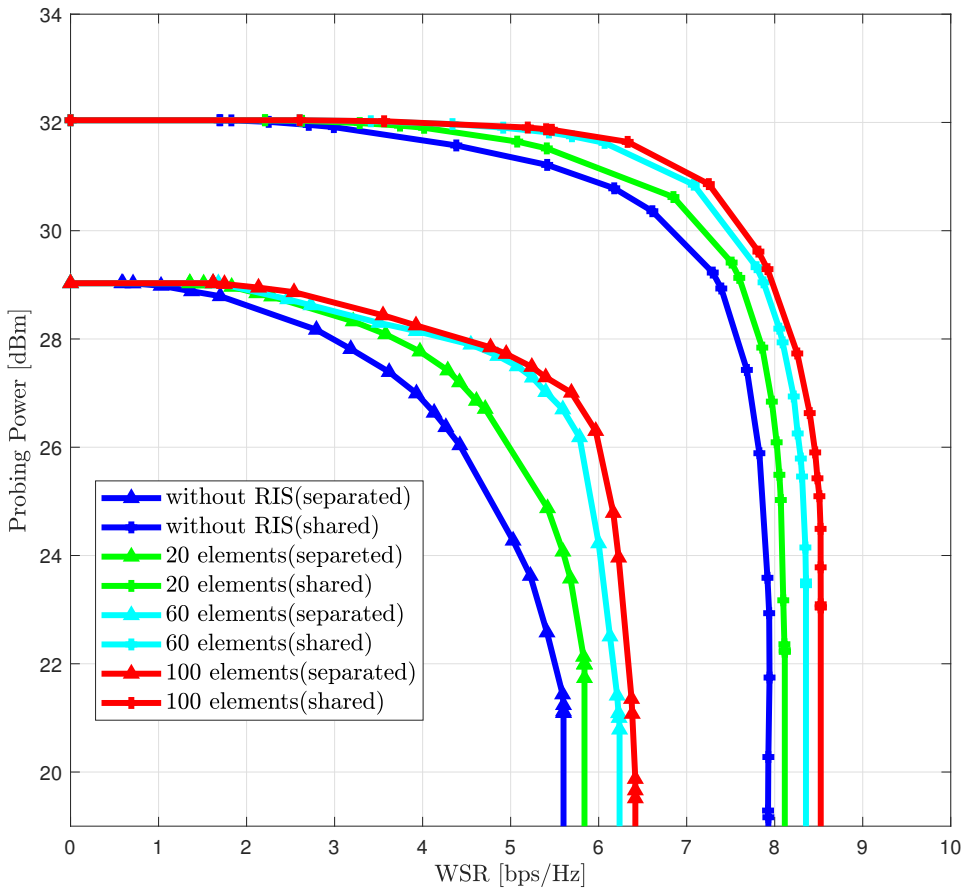

Figure 4.9: Effect of the number of reflecting elements on tradeoff in Rayleigh channels

Chapter 5

Conclusions and Future Work

This paper presented the detailed beamforming optimization for RIS-aided DFRC system. Unlike existing works, this is the first work that investigates the maximization of WSR and probing power. Two AO algorithms based on WMMSE and FP are proposed to solve the non-convex optimization problems for active and passive beamforming in seperated and shared deployments. The applied RIS model is not limited to the widely-used single connected model, but extended to a generalized group or fully connected RIS model.

The simulation results validated the proposed algorithm's effectiveness and led to the following findings.

1. In both separated and shared deployments, the RIS aids the system in achieving improved radar beampatterns and larger achievable region of WSR and probing power.

2. Compared with separated deployment, the shared deployment achieves significantly better beampattern and tradeoff because the antennas are fully exploited.

3. The fully connected RIS brings more improvements in terms of radar beampattern and achievable region than single connected RIS in Rayleigh channel, while its performance is the same as single connected RIS in LOS channel.

4. With the increase of the number of reflecting elements at RIS, the achievable region becomes larger but asymptotically reaches an upper limit.

5. Although the higher upper bound of WSR is achieved by RIS, the upper bound of probing power remains unchanged. The reason is that the probing power is totally determined by BS and therefore RIS essentially makes no difference.

Some limitations in this project are valuable for future consideration.

1. The gains of both beampattern and achievable region from RIS are essentially due to the upgrade of communication performance instead of radar performance or both.

2. The algorithm using scattering-reactance relationship to optimize group or fully connected RIS converges slow, which is quite impractical.

3. Compared to more representative metrics like detection and false-alarm probability, probing power is a simplistic metric to assess a radar performance.

As RIS is only related to the channel between BS, users and radar targets, the radar metrics related to the channel should be chosen in order to obtain gain from RIS. The conventional radar metrics including detection probability, false-alarm probability, and mean square error are good candidates. However, as mentioned in Section 2.2.2, these metrics are difficult to optimize. One potential solution is machine learning techniques, which have attracted much attention in RIS research due to their learning capability and large search-space [1]. For example, in both [43] and [44], the achievable rate is set as reward and maximized by reinforcement learning model. Therefore, although the metrics are complicated, the optimal solution may be found by designing a machine learning model properly, which is one of future research opportunities.

Appendix A

Source Code

The source code of simulation can be retrieved from [this link].

Bibliography

[1] Y. Liu, X. Liu, X. Mu, T. Hou, J. Xu, M. Di Renzo, and N. Al-Dhahir, "Reconfigurable intelligent surfaces: Principles and opportunities," *IEEE Communications Surveys Tutorials*, pp. 1–1, 2021.

[2] S. Shen, B. Clerckx, and R. Murch, "Modeling and architecture design of intelligent reflecting surfaces using scattering parameter network analysis," *arXiv preprint arXiv:2011.11362*, 2020.

[3] F. Liu, C. Masouros, A. P. Petropulu, H. Griffiths, and L. Hanzo, "Joint radar and communication design: Applications, state-of-the-art, and the road ahead," *IEEE Transactions on Communications*, vol. 68, no. 6, pp. 3834–3862, 2020.

[4] F. Liu and C. Masouros, "A tutorial on joint radar and communication transmission for vehicular networks-part i: Background and fundamentals," *IEEE Communications Letters*, 2020.

[5] Z. Feng, Z. Fang, Z. Wei, X. Chen, Z. Quan, and D. Ji, "Joint radar and communication: A survey," *China Communications*, vol. 17, no. 1, pp. 1–27, 2020.

[6] H. Guo, Y.-C. Liang, J. Chen, and E. G. Larsson, "Weighted sum-rate maximization for intelligent reflecting surface enhanced wireless networks," in *2019 IEEE Global Communications Conference (GLOBECOM)*. IEEE, 2019, pp. 1–6.

[7] Q. Wu and R. Zhang, "Intelligent reflecting surface enhanced wireless network via joint active and passive beamforming," *IEEE Transactions on Wireless Communications*, vol. 18, no. 11, pp. 5394–5409, 2019.

[8] H. Guo, Y.-C. Liang, J. Chen, and E. G. Larsson, "Weighted sum-rate maximization for reconfigurable intelligent surface aided wireless networks," *IEEE Trans. Wireless Commun.*, vol. 19, no. 5, pp. 3064–3076, 2020.

[9] C. Xu, B. Clerckx, and J. Zhang, "Multi-antenna joint radar and communications: Precoder optimization and weighted sum-rate vs probing power tradeoff," *IEEE Access*, vol. 8, pp. 173 974–173 982, 2020.

[10] M. Rihan and L. Huang, "Optimum co-design of spectrum sharing between mimo radar and mimo communication systems: An interference alignment approach," *IEEE Transactions on Vehicular Technology*, vol. 67, no. 12, pp. 11 667–11 680, 2018.

[11] J. Qian, M. Lops, L. Zheng, X. Wang, and Z. He, "Joint system design for coexistence of mimo radar and mimo communication," *IEEE Transactions on Signal Processing*, vol. 66, no. 13, pp. 3504–3519, 2018.

[12] B. Li, A. P. Petropulu, and W. Trappe, "Optimum co-design for spectrum sharing between matrix completion based mimo radars and a mimo communication system," *IEEE Transactions on Signal Processing*, vol. 64, no. 17, pp. 4562–4575, 2016.

[13] B. Li and A. P. Petropulu, "Joint transmit designs for coexistence of mimo wireless communications and sparse sensing radars in clutter," *IEEE Transactions on Aerospace and Electronic Systems*, vol. 53, no. 6, pp. 2846–2864, 2017.

[14] F. Liu, C. Masouros, A. Li, T. Ratnarajah, and J. Zhou, "Mimo radar and cellular coexistence: A power-efficient approach enabled by interference exploitation," *IEEE Transactions on Signal Processing*, vol. 66, no. 14, pp. 3681–3695, 2018.

[15] S. Sodagari, A. Khawar, T. C. Clancy, and R. McGwier, "A projection based approach for radar and telecommunication systems coexistence," in *2012 IEEE Global Communications Conference (GLOBECOM)*. IEEE, 2012, pp. 5010–5014.

[16] J. A. Mahal, A. Khawar, A. Abdelhadi, and T. C. Clancy, "Spectral coexistence of mimo radar and mimo cellular system," *IEEE Transactions on Aerospace and Electronic Systems*, vol. 53, no. 2, pp. 655–668, 2017.

[17] H. Deng and B. Himed, "Interference mitigation processing for spectrum-sharing between radar and wireless communications systems," *IEEE Transactions on Aerospace and Electronic Systems*, vol. 49, no. 3, pp. 1911–1919, 2013.

[18] G. Meager, R. A. Romero, and Z. Staples, "Estimation and cancellation of high powered radar interference for communication signal collection," in *2016 IEEE Radar Conference (RadarConf)*. IEEE, 2016, pp. 1–4.

[19] N. Nartasilpa, S. Shahi, A. Salim, D. Tuninetti, N. Devroye, D. Erricolo, D. P. Zilz, and M. R. Bell, "Let's share commrad: Co-existing communications and radar systems," in *2018 IEEE Radar Conference (RadarConf18)*. IEEE, 2018, pp. 1278–1283.

[20] A. Hassanien, M. G. Amin, E. Aboutanios, and B. Himed, "Dual-function radar communication systems: A solution to the spectrum congestion problem," *IEEE Signal Processing Magazine*, vol. 36, no. 5, pp. 115–126, 2019.

[21] A. Hassanien, B. Himed, and M. G. Amin, "Transmit/receive beamforming design for joint radar and communication systems," in *2018 IEEE Radar Conference (RadarConf18)*. IEEE, 2018, pp. 1481–1486.

[22] X. Liu, T. Huang, N. Shlezinger, Y. Liu, J. Zhou, and Y. C. Eldar, "Joint transmit beamforming for multiuser mimo communications and mimo radar," *IEEE Transactions on Signal Processing*, vol. 68, pp. 3929–3944, 2020.

[23] F. Liu, C. Masouros, A. Li, J. Zhou, and L. Hanzo, "Simultaneous target detection and multi-user communications enabled by joint beamforming," in *2018 IEEE Radar Conference (RadarConf18)*. IEEE, 2018, p. 89.

[24] K. Shen and W. Yu, "Fractional programming for communication systems—part i: Power control and beamforming," *IEEE Transactions on Signal Processing*, vol. 66, no. 10, pp. 2616–2630, 2018.

[25] ——, "Fractional programming for communication systems—part ii: Uplink scheduling via matching," *IEEE Transactions on Signal Processing*, vol. 66, no. 10, pp. 2631–2644, 2018.

[26] W. Lu, B. Deng, Q. Fang, X. Wen, and S. Peng, "Intelligent reflecting surface-enhanced target detection in mimo radar," *IEEE Sensors Letters*, vol. 5, no. 2, pp. 1–4, 2021.

[27] S. Buzzi, E. Grossi, M. Lops, and L. Venturino, "Radar target detection aided by reconfigurable intelligent surfaces," *IEEE Signal Processing Letters*, 2021.

[28] A. Aubry, A. De Maio, and M. Rosamilia, "Reconfigurable intelligent surfaces for n-los radar surveillance," *arXiv preprint arXiv:2104.00456*, 2021.

[29] S. Buzzi, E. Grossi, M. Lops, and L. Venturino, "Foundations of mimo radar detection aided by reconfigurable intelligent surfaces," *arXiv preprint arXiv:2105.09250*, 2021.

[30] X. Wang, Z. Fei, J. Guo, Z. Zheng, and B. Li, "Ris-assisted spectrum sharing between mimo radar and mu-miso communication systems," *IEEE Wireless Communications Letters*, vol. 10, no. 3, pp. 594–598, 2020.

[31] Z.-M. Jiang, M. Rihan, P. Zhang, L. Huang, Q. Deng, J. Zhang, and E. M. Mohamed, "Intelligent reflecting surface aided dual-function radar and communication system," *IEEE Systems Journal*, pp. 1–12, 2021.

[32] X. Wang, Z. Fei, Z. Zheng, and J. Guo, "Joint waveform design and passive beamforming for ris-assisted dual-functional radar-communication system," *IEEE Transactions on Vehicular Technology*, 2021.

[33] Z.-Q. Luo, W.-K. Ma, A. M.-C. So, Y. Ye, and S. Zhang, "Semidefinite relaxation of quadratic optimization problems," *IEEE Signal Processing Magazine*, vol. 27, no. 3, pp. 20–34, 2010.

[34] D. Tse and P. Viswanath, *Fundamentals of wireless communication*. Cambridge university press, 2005.

[35] B. Clerckx and C. Oestges, *MIMO wireless networks: channels, techniques and standards for multi-antenna, multi-user and multi-cell systems*. Academic Press, 2013.

[36] P. Stoica, J. Li, and Y. Xie, "On probing signal design for mimo radar," *IEEE Transactions on Signal Processing*, vol. 55, no. 8, pp. 4151–4161, 2007.

[37] R. Schmidt, "Multiple emitter location and signal parameter estimation," *IEEE transactions on antennas and propagation*, vol. 34, no. 3, pp. 276–280, 1986.

[38] S. Liu, Z. Gao, J. Zhang, M. Di Renzo, and M.-S. Alouini, "Deep denoising neural network assisted compressive channel estimation for mmwave intelligent reflecting surfaces," *IEEE Transactions on Vehicular Technology*, vol. 69, no. 8, pp. 9223–9228, 2020.

[39] A. M. Elbir, A. Papazafeiropoulos, P. Kourtessis, and S. Chatzinotas, "Deep channel learning for large intelligent surfaces aided mm-wave massive mimo systems," *IEEE Wireless Communications Letters*, vol. 9, no. 9, pp. 1447–1451, 2020.

[40] S. S. Christensen, R. Agarwal, E. De Carvalho, and J. M. Cioffi, "Weighted sum-rate maximization using weighted mmse for mimo-bc beamforming design," *IEEE Transactions on Wireless Communications*, vol. 7, no. 12, pp. 4792–4799, 2008.

[41] M. Grant and S. Boyd, "CVX: Matlab software for disciplined convex programming, version 2.1," http://cvxr.com/cvx, Mar. 2014.

[42] 3GPP, "Evolved Universal Terrestrial Radio Access (E-UTRA); Further advancements for E-UTRA physical layer aspects," 3rd Generation Partnership Project (3GPP), Technical Specification (TS) 36.814, 2015. [Online]. Available: https://portal.3gpp.org/desktopmodules/Specifications/SpecificationDetails.aspx?specificationId=2493

[43] C. Huang, R. Mo, and C. Yuen, "Reconfigurable intelligent surface assisted multiuser miso systems exploiting deep reinforcement learning," *IEEE Journal on Selected Areas in Communications*, vol. 38, no. 8, pp. 1839–1850, 2020.

[44] A. Taha, Y. Zhang, F. B. Mismar, and A. Alkhateeb, "Deep reinforcement learning for intelligent reflecting surfaces: Towards standalone operation," in *2020 IEEE 21st International Workshop on Signal Processing Advances in Wireless Communications (SPAWC)*. IEEE, 2020, pp. 1–5.